Modelling early warning signals for critical transitions in a water-controlled grazing system

MSc graduation research

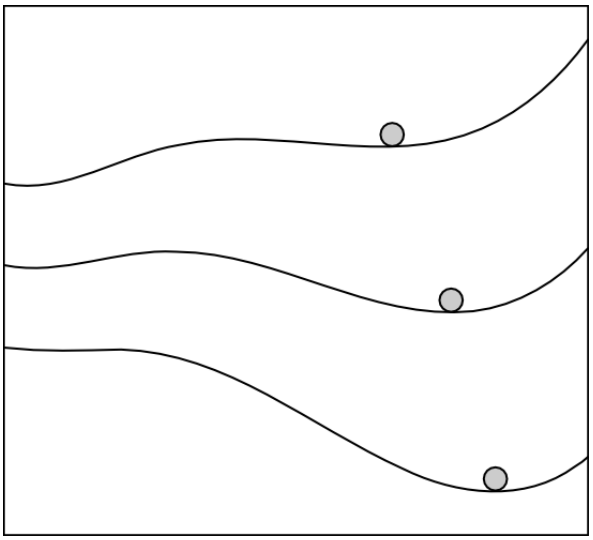

Date: April 2, 2011
By: Koen Siteur (3169987)
Programme: Hydrology, Utrecht University
Track: Earth Surface Hydrology

Supervision: Derek Karssenberg
Marc Bierkens

Modelling early warning signals for critical transitions in a water-controlled grazing system.

Course:
MSc graduation research (GEO4-1520)

Date:
April 2, 2011

By:
Koen Siteur (3169987)
06-19435813
k.siteur@gmail.com
k.siteur@students.uu.nl

Supervision:
Derek Karssenberg

Co-supervision:
Marc Bierkens

Programme:
Hydrology, Utrecht University

Track:
Earth Surface Hydrology

Abstract

In systems subject to gradually changing conditions abrupt and sometimes irreversible shifts between two stable states can take place if a certain threshold is exceeded. These so called critical transitions also occur in arid ecosystems subject to grazing or changing climatic conditions. The transition from a vegetated to a barren state is problematic as it plays a key role in global desertification. Fortunately, early warning signals for this transition in the form of vegetation patterns can often be observed in these ecosystems. In addition, more general signals related to the principle of critical slowing down may be found, as they appear in many systems that approach a transition. This study aims to gain more insight in the behaviour of arid ecosystems and the early warning signals that may be found in these systems.

A model was developed and evaluated on early warning signals. The main transition in this model is based on feedbacks between grazing and vegetation growth. When grazing exceeds vegetation growth, the systems collapses. This type of transition was studied before, but in this model water – the resource that was assumed to limit vegetation growth – is explicitly modelled. This allows spatial hydrological processes to be modelled and enables the transition to be forced with hydrological parameters like rainfall intensity and frequency. Furthermore, early warning signals for the transition may be detected in the hydrological compartments of the model.

For the transition in this system early warning signals in vegetation density can be found in the form of decreasing skewness and increasing variance and correlation. These signals can be found both in spatial data and time series data. Depending on the relation between vegetation density and infiltration, the signals can also be found in time series of annual discharge, with exception of changing skewness. The variability of the climate however, may result in a weakening of the trends in these indicators. Furthermore, the signals can also be observed when the transition is gradual. Changes in precipitation are less likely to cause a shift in the modelled system compared to intensified grazing. Besides the shift induced by grazing-growth feedbacks another transition is hidden in this system. Feedbacks related to interactions between vegetation and its limiting resource are responsible for this second transition and result in self-organisation of vegetation in vegetation bands. These bands may also serve as early warning signals for this transition. It was hypothesized that the formation of vegetation bands depends both on soil properties and variability in climate and vegetation cover.

Table of contents

1 Introduction

In systems subject to gradually changing conditions abrupt and sometimes irreversible shifts between two stable states can take place if a certain threshold (critical point/bifurcation point) is exceeded. These so called critical transitions occur in many systems, ranging from financial markets to the human body (Scheffer et al., 2009).

Critical transitions can also be found in hydrological systems, especially if vegetation is part of the system. In these ecosystems, often located in dry areas, small changes in grazing or precipitation can result in a sudden transition from a vegetated state to a barren state. The irreversible nature of this transition is problematic as it plays a key role in global desertification, which affects millions of lives in mainly underdeveloped countries.

Model studies in the second part of the twentieth century significantly improved our knowledge about transitions in arid ecosystems. In general, shifts in vegetation cover occur due to non-linear behaviour of the system. This non-linear behaviour is often modelled using feedbacks within the resource-vegetation system (e.g. Rietkerk, 1997), but also models that only cover grazing and growth of vegetation can result in a transition (e.g. May, 1977). When a transition is modelled using resource feedback mechanisms (so feedbacks within the resource-vegetation system) it is often assumed that, to some level, vegetation has a positive effect on its own limiting resource. For example, in models made by Rietkerk et al. (1997), vegetation allows more water to infiltrate or prevents soil nutrient erosion. The non-linear behaviour is then caused by the fact that vegetation both consumes and harvests/protects its own resource. May (1977) however, does not dedicate vegetation shifts to this mechanism, but showed that shifts can occur in systems with logistically growing vegetation, when grazing exceeds growth.

Although the models described above increased our knowledge about shifts in vegetation cover, they cannot be used to predict shifts as they are not developed for that purpose. However, empirical and physically based models that were made for estimating the impact of grazing or climate on this type of ecosystems do not generate satisfactory results when it comes to predicting shifts (e.g. WEBB, 1995; EPIC, 1995).

A more recent conceptual model by Rietkerk et al. (2002) however, shows that it is often not necessary to predict shifts using comprehensive models, as clear spatial patterns emerge far before the transition from a vegetated to a barren state takes place (figure 1.1). These indicators, often referred to with the term 'early warning signals', can be found in various arid ecosystems. More recently, Scheffer et al. (2009) published a paper in which early warning signals were reviewed. It appears that some signals can in theory be found in a large variety of systems. Increasing autocorrelation and variance are indicators that can be found in systems approaching a transition, as well as changes in skewness and flickering between two stable states (Scheffer et al., 2009).

Using May's overharvesting model (1977) it can be shown that the general early warning signals reviewed by Scheffer et al. (2009) can as well emerge in grazing systems (Dakos, 2009; Karssenberg & Bierkens, 2010). However, transition models that explicitly include hydrology were never evaluated for these signals. In addition, hydrological processes in these models are often poorly represented. The stochastic nature of the intensity and frequency of rain events, for example, may play a significant role in the formation of patterns or can affect the more general signals that may emerge. Furthermore, if hydrology is modelled in more detail, indicators for transitions may be found in hydrological variables like soil moisture or discharge instead of vegetation cover. In addition, parameters other than grazing or annual rainfall, such as rainfall frequency or intensity, can then be used when forcing the system to undergo a transition[1]. How would such a system behave and what early warning signals will appear?

In this report a model is presented in which grazing, vegetation growth and hydrology are represented in a simple but realistic way. The feedback mechanism behind the transition in this model is derived from the overharvesting model of May (1977). The model is evaluated for early warning signals and its behaviour is analysed to answer the following questions:

[1] Parameters used to force a transition will be revered to as 'driver' hereafter.

- How does the model behave?
- What early warning signals appear for the transition in this model?
- In what components of the model do these early warning signals appear?
- How does the model behaviour and how do the early warning signals found depend on the driver used?
- How does the model behaviour and how do the early warning signals found depend on the parameter setting used?

It is hypothesized that using the feedbacks in May's overharvesting model, a transition can be created regardless of the driver used. Increasing the grazing rate will result in a transition if grazing exceeds vegetation growth. The same can be obtained if the vegetation growth declines due to changes in rainfall frequency or intensity. General early warning signals, described by Scheffer et al. (2009), are expected to be detected in spatial and temporal data, independent of the driver used. They are expected to be present in vegetation density maps and time series as well as temporal data of annual discharge.

The remainder of this report is structured as follows. First some theoretical background is given to fully understand the principles behind critical transitions and early warning signals (chapter 2). In chapter 3, methodology, the shift in this particular model is explained and a model description is given. The evaluation of the model output on early warning signals and the different scenarios are explained in this chapter as well. The results are presented in chapter 4. In chapter 5 the results are discussed and from this conclusions are drawn in chapter 6.

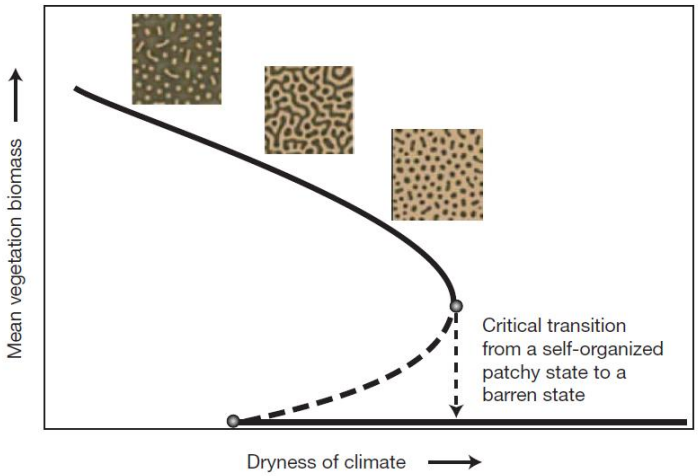

Figure 1.1: Before the critical transition from a vegetated state to a barren state takes place, clear spatial patterns appear. Solid lines: stable equilibria (attractors). Dashed line: unstable equilibrium. Light colour: bare soil. Dark colour: vegetation. (Rietkerk et al., 2004; modified)

2 Theoretical background

2.1 Types of transitions

Before discussing the nature of early warning signals and the feedbacks responsible for critical transitions in arid ecosystems, one should be familiar with the different types of transitions (figure 2.1). A transition in a system is induced by an external forcing, so changing conditions. If a system behaves more or less linear, which is often the case, a large external change is needed to force a transition (figure 2.1a). However, it can be that a small change in conditions results in a big change in system state (a critical transition; figure 2.1b-c). If the same system state cannot be obtained when conditions are changed back to the initial situation (figure 2.1c), this is called a catastrophic transition.

Catastrophic transitions can be the result of changing conditions, but may as well be caused by perturbations in system state that force it out of its basin of attraction (figure 2.1d; Scheffer et al., 2009). Catastrophic shifts can be found in various systems and are a popular research topic, because of their irreversible and therefore often problematic nature.

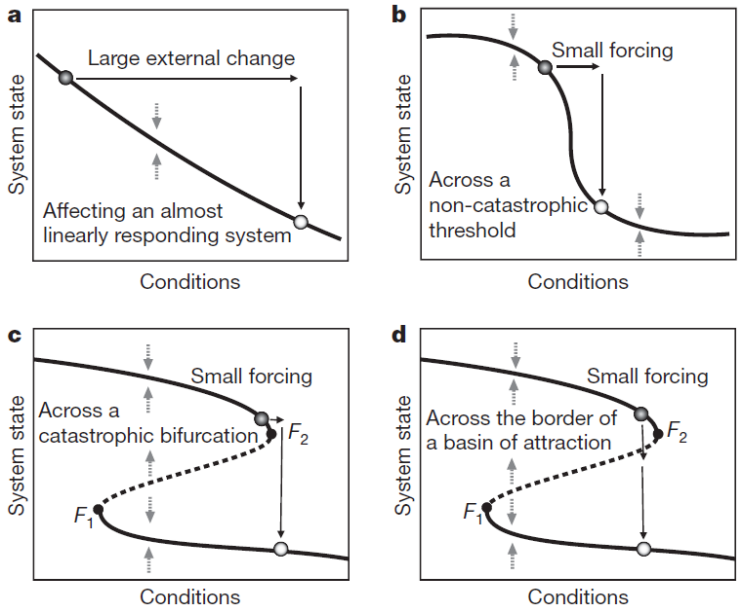

Figure 1.2. The four different types of transitions. Solid lines: stable equilibria. Dashed lines: unstable equilibria. (Scheffer, 2009)

2.2 Generic early warning signals

The patterns that were found by the model of Rietkerk et al. (2002) (figure 1.1), can be found in a variety of ecosystems (from arid areas to peatlands; Rietkerk et al., 2004), but are still rather specific early warning signals. More general signals, discussed in a review by Scheffer et al. (2009), are often related to the principle of 'critical slowing down'. When a system approaches a critical point it becomes increasingly slow in recovering from perturbations. In other words, the stability of the system gets lower (see Scheffer et al., 2009, box 2 for theoretical background). It can be proven that this phenomenon occurs in any continuous model approaching a catastrophic transition (figure 2.1c-d; Wissel, 1984).

In small systems, that can be isolated so that one controls all external conditions, it is possible to perturb it to measure the recovery time and thereby obtain information about the timing of a transition. For most systems, however, this is not possible. Fortunately, these systems are often subject to natural perturbations. As systems become increasingly slow in recovering from these perturbations, the state of a system at any given moment becomes more like its past state. This results in an increase in autocorrelation in timeseries (Ives, 1995). Increasing autocorrelation is directly linked to critical slowing down and is therefore considered as the most important predictor for critical transitions in natural systems (Scheffer et al., 2009).

Another early warning signal related to critical slowing down is increasing variance. When the recovery rate of a system drops, perturbations have an accumulating effect which causes the variability within the system to increase. This, however, does not have to be true as critical slowing down can as well reduce the response rate and thereby the ability of the system to track the fluctuations (Scheffer et al., 2009).

A third general early warning signal that can be found in systems with a folded equilibrium curve are changes in skewness caused by increasing asymmetry in recovery rate. As shown in figures 1.1 and 2.1c-d, an unstable equilibrium approaches the attractor from one side when the system moves in the direction of a critical transition. Near this unstable equilibrium rates of change are lower, leading to a change in skewness in frequency distributions (Guttal & Jayaprakash, 2008).

Flickering is an early warning signal for transitions in systems with strong natural perturbations. In these systems, stochastic forcing is strong enough to move the system from one stable state to the other and back. Bimodality in frequency distributions is an indicator for flickering (Scheffer et al., 2009).

In addition to the indicators that can be found in time series data, maps can obtain information about upcoming transitions. For example, Dakos et al. (2009) showed for three different systems containing reaction and diffusion processes that increasing spatial correlation is often a better indicator for critical transitions than increasing autocorrelation in time series.

2.3 Transitions in arid grazing systems

Transitions in arid grazing systems can be caused by numerous feedbacks. What we observe is that vegetation does not survive if vegetation density becomes lower than a certain threshold value. From this observation, one could state that vegetation growth is negative at low vegetation densities. Negative growth at low vegetation densities can have several causes, but in model studies it is often assumed that the cause is either related to resource or grazing feedback mechanisms. Models based on resource feedback mechanisms assume that vegetation has in some way a positive effect on the resource that limits growth. Vegetation can for example increase the permeability of the soil so that more water infiltrates or it can prevent erosion of nutrients (Rietkerk et al., 1997). Depending on the parameter setting used, this can lead to a non linear behaviour of the system and thereby to critical transitions (Rietkerk et al., 1997). May's overharvesting model is a model that dedicates the shift to grazing instead of resource feedback mechanisms. If grazing exceeds the maximum vegetation growth, the system collapses. A more detailed description of May's overharvesting model can be found in section 3.1.1.

3 Methodology

3.1 Model description

To be able to study early warning signals for critical transitions in a water-controlled grazing system, the modelled system should obviously contain a critical transition. The feedbacks in the model, which is called WOTMOD (water-controlled overgrazing transition model), are therefore based on the overharvesting model of May (1977), as it is known that this model contains a critical transition and that early warning signals appear (increasing temporal and spatial correlation) when the system approaches this transition (Dakos et al., 2009; Karssenberg & Bierkens, 2010).

3.1.1 May's overharvesting model

May's overharvesting model (1977) describes the vegetation density only and consists of one differential equation with a growback term and a grazing term:

$$\frac{dV}{dt} = rV(1 - \frac{V}{K}) - g\frac{V^2}{V^2 + \alpha^2} \qquad (1)$$

In equation 1, V is the vegetation density [kg/m^2], r is the growth rate [y^{-1}], K is the carrying capacity [kg/m^2], g is the grazing rate [kg/m^2/y] and α is the vegetation density where the grazing is ½g [kg/m^2].

If one plots the two terms of equation 1 against vegetation density, figure 3.1 can be obtained. At low vegetation densities, vegetation growth rises as vegetation density increases, at higher vegetation densities however, vegetation growth decreases again. Competition between individual plants explains the shape of this curve. At low vegetation densities, there is hardly any competition. In this stage, the accumulation of biomass could for example be limited by the rate of photosynthesis that takes place, which is related to the available leaf area. This in turn is related to the biomass, which explains why an increase in vegetation density leads to a higher vegetation growth. However, as vegetation becomes denser, competition for resource(s), like sunlight, nutrients or water, becomes more important. This is why growth is then limited and even becomes zero when the carrying capacity (K) is reached. The second term in equation 1 (grazing) is a saturation function (see appendix B) that has a value of g at high vegetation densities. At lower densities, grazing drops.

The shift that occurs in this system can be caused by a gradual increase in grazing rate (g). Figure 3.1 shows that three stages can be distinguished while the grazing rate increases. At low grazing rates (stage 1), there is only one stable equilibrium. These low grazing rates are sustainable because no transition can take place as long as there is only one stable state. When the grazing rate increases (stage 2), another stable state emerges at a lower vegetation density. At this stage, transitions between the two stable states can take place, as perturbations in any of the parameters can force the system out of one basin of attraction into the other (see also figure 2.2). When the grazing rate increases even more, there is again only one stable equilibrium (stage 3). However, this equilibrium is situated at a much lower vegetation density than the one of stage 1.

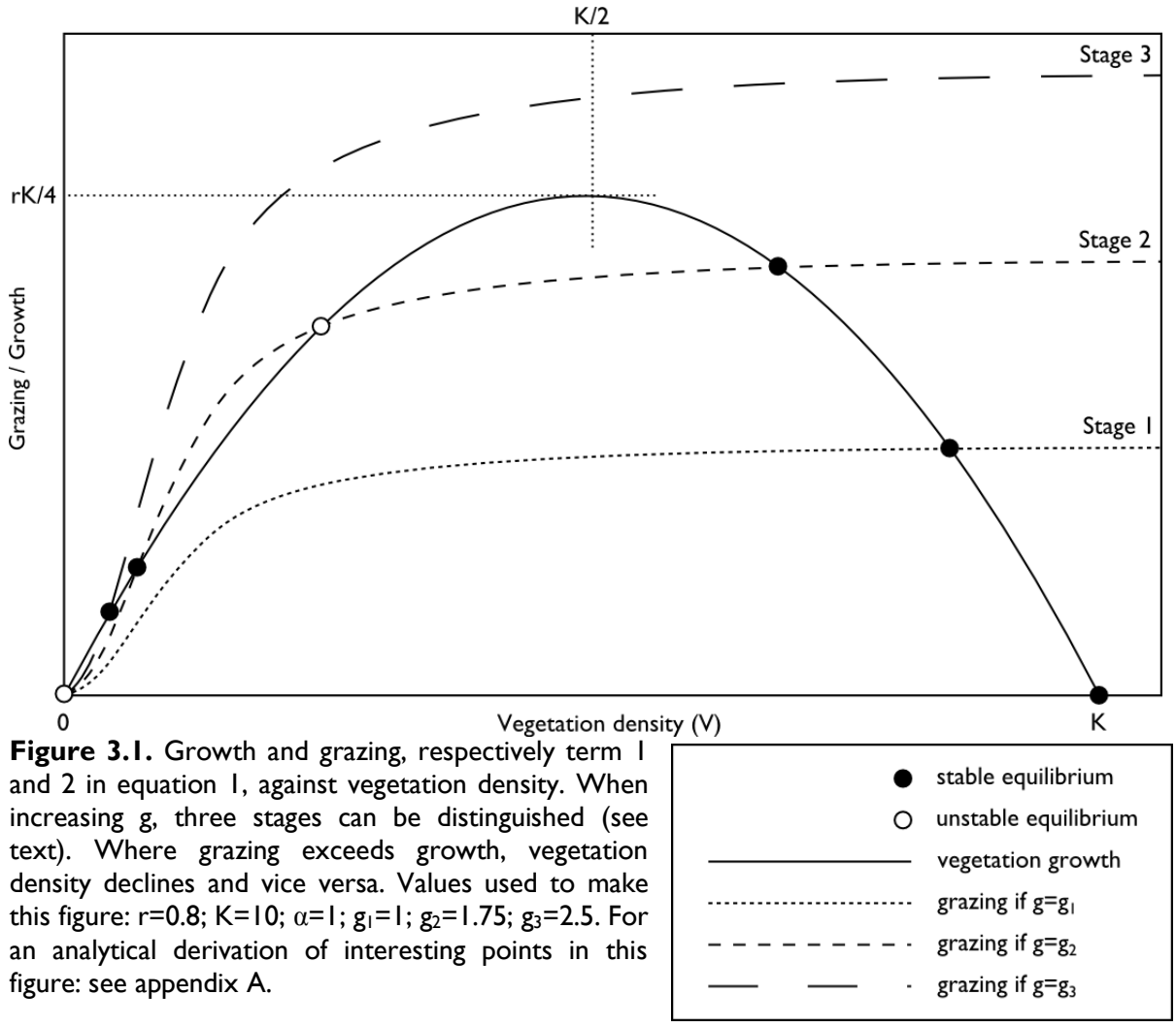

Figure 3.1. Growth and grazing, respectively term 1 and 2 in equation 1, against vegetation density. When increasing g, three stages can be distinguished (see text). Where grazing exceeds growth, vegetation density declines and vice versa. Values used to make this figure: r=0.8; K=10; α=1; g_1=1; g_2=1.75; g_3=2.5. For an analytical derivation of interesting points in this figure: see appendix A.

In systems like the one modelled by May (1977), early warning signals related to critical slowing down can be found (Dakos et al., 2009; Karssenberg & Bierkens, 2010). As discussed before, this means that the system becomes increasingly slow in recovering from perturbations when it approaches a transition, as the eigenvalues characterizing the rates of change near the stable equilibrium tend to zero (Scheffer et al., 2009). An easier way to show what happens when the system approaches a transition is by integrating equation 1 with respect to V, as shown in figure 3.2.

At low grazing rates, the recovery rate is high. In other words, the system can recover relatively quickly from perturbations in vegetation density. Furthermore the basin of attraction is wide, implying that very big perturbations are needed to force the system out of its current state. When the grazing rate increases, the basin of attraction gets narrower and the recovery rate drops. Not only does the recovery rate drop, it also becomes asymmetrical. Perturbations to the right in figure 3.2 (higher vegetation density) have a minor effect as the system recovers quickly, while the system needs more time to recover from perturbations towards lower vegetation densities.

This has implications for early warning signals that can appear in systems like the one modelled by May (1977). A lowering in recovery rate will lead to an increase in autocorrelation in vegetation density, because the state of the system at a given moment in time becomes more and more like its past states. A lower recovery rate will also lead to a greater variability in vegetation density, as perturbations accumulate. A decrease in skewness in frequency distribution can be expected as the system recovers slower from perturbations towards lower vegetation densities. Finally, the narrowing of the basin of attraction can result in flickering between the two stable equilibria. These findings are consistent with the signals discussed in the review by Scheffer et al. (2009).

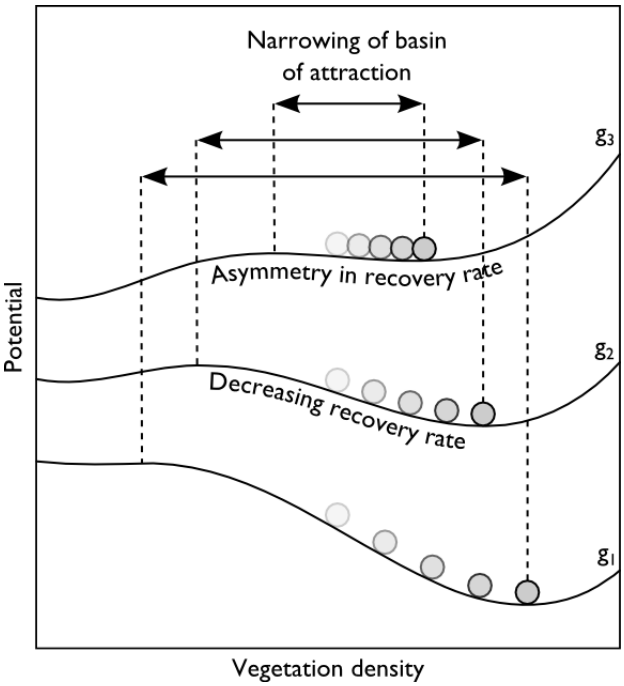

Figure 3.2. Stability landscapes of May's overharvesting model for different grazing rates against vegetation density. Potential=-∫f(V) from 0 to V, with f(V)=dV/dt, so the slope of the lines represents the net growth: a negative slope implies a positive net growth and vice versa. At the equilibria, the net growth is zero. The state of the system is represented by the marble. Values used to make this figure: r=0.8; K=10; α=1; g_1=1.5, g_2=1.75 and g_3=2.

3.1.2 WOTMOD

The feedbacks that are responsible for the transition in WOTMOD are similar to the feedbacks in May's overharvesting model (1977). However, the not defined resource that limits vegetation growth near carrying capacity is now explicitly modelled in the form of water using a second state variable (soil saturation; S). Modelling water separately allows us to force a shift with parameters other than grazing rate, like rainfall intensity or frequency. Furthermore, spatial processes can be modelled, including overland flow. Finally, signals may be found in other variables than vegetation density, like soil saturation or surface runoff.

Unlike May's model, WOTMOD is a distributed model. In a lattice of m·n cells, each cell (i,j) represents a subsystem that is described by the equations in this section. The differential equations presented are solved explicitly using a weekly timestep. Model output consists of annual vegetation density maps and discharge maps that are later evaluated for early warning signals (see section 3.3). The model is made using MATLAB 2009b (Mathworks). The model script can be found in appendix C.I.

3.1.2.1 Soil water fluxes

In WOTMOD, the change in moisture content of the rootzone is described by:

$$nZ_r \frac{dS_{i,j}}{dt} = I_{i,j} - S_{i,j}^u E_{max} \frac{V_{i,j} + \beta V_0}{V_{i,j} + \beta} \quad (2)$$

with:

$$S_{i,j} = \frac{\theta_{i,j} - \theta_r}{\theta_{sat} - \theta_r}$$

In equation 2, the first term represents the infiltration of water into the rootzone (described in section 3.1.2.3) and the second term the evapotransiration from the rootzone. $S_{i,j}$ is the saturation of the rootzone [-], t is time [y], Z_r is the depth of the rootzone [m], n is the porosity (θ_{sat}-θ_r) [-], $\theta_{i,j}$ is the volumetric moisture content in the soil [-], θ_r is the residual moisture content [-], θ_{sat} is the moisture content at saturation [-], $I_{i,j}$ is the infiltration [m/year], u relates evapotranspiration to soil saturation [-], E_{max} is the evapotranspiration from a fully vegetated saturated soil [m/year], $V_{i,j}$ is the vegetation density [kg/m^2], V_0 is the evapotranspiration from bare soil as fraction of $E_{max}S^u$ [-] and β is a saturation constant relating evapotranspiration to vegetation density [kg/m^2].

The saturation of the rootzone ($S_{i,j}$) has a value between 0 and 1. When $S_{i,j}$ is 0, the moisture content of the rootzone ($\theta_{i,j}$) equals the residual moisture content (θ_r). If $S_{i,j}$=1, the soil is saturated. It is assumed that plants can take up moisture till $\theta_{i,j} = \theta_r$. The fluxes, infiltration and evapotranspiration, are both in m/year, which is why $S_{i,j}$ is multiplied by the depth of the rootzone (Z_r, in m) and the porosity (n).

The evapotranspiration [m/y], the second term in equation 2, depends both on vegetation density and saturation of the rootzone. Its dependence on vegetation density is represented by a saturation function (see appendix B). If the soil is completely saturated and the vegetation density is infinite, the evapotranspiration equals E_{max}. From a not vegetated saturated soil, evaporation is $V_0 \cdot E_{max}$. One can subdivide evapotranspiration in soil evaporation and transpiration by plants as shown in appendix B. The relationship between evapotranspiration and soil saturation follows: $S_{i,j}^u$ (Entekhabi et al., 1992).

Interception and percolation fluxes are assumed to be negligible compared to the infiltration and evapotranspiration fluxes and are therefore not modelled.

3.1.2.2 Vegetation growth and grazing

The change in vegetation density is modelled using a revised version of May's model (equation 3). Growth is represented by the first two terms and grazing by the third term. The fourth and fifth terms are a dispersion and a noise term respectively. These two terms were added to May's model before with the aim to model spatial early warning signals, e.g. Dakos et al. (2008) and Karssenberg & Bierkens (2010).

$$\frac{dV_{i,j}}{dt} = cS_{i,j}^u E_{max} \frac{V_{i,j}}{V_{i,j} + \beta} - dV_{i,j} - g \frac{V_{i,j}^2}{V_{i,j}^2 + \alpha^2} + D(V_{i,j+1} + V_{i,j-1} + V_{i+1,j} + V_{i-1,j} - 4V_{i,j}) + \sigma_W W_{i,j} \quad (3)$$

In equation 3, c is the water use efficiency [kg/m^3], β is the half-saturation constant relating transpiration by plants to vegetation density[2] [kg/m^2], d it the maintenance rate [y^{-1}], g is the grazing rate [kg/m^2/y], α is the half-saturation constant relating grazing to vegetation density [kg/m^2], D is the dispersion rate [y^{-1}], σ_w is the standard deviation of the white noise [kg/m^2] and $W_{i,j}$ is normally distributed white noise uncorrelated in space and time.

Plant transpiration and photosynthesis are often strongly coupled (Daly et al., 2004). In WOTMOD vegetation growth is linearly related to the amount of water that is transpired, using water use efficiency, c. Part of the energy captured by photosynthesis is used for maintenance of the

[2] Note that the half-saturation constants that relate evapotranspiration and transpiration to vegetation density are assumed to be equal (β).

plants (dV). Grazing is modelled as in May's overharvesting model and declines when vegetation density gets lower.

WOTMOD is expected to behave like May's model, as its feedbacks are similar. Vegetation growth increases as vegetation density increases, due to an increasing photosynthesis/transpiration. At higher vegetation densities more water is lost by transpiration and growth is limited by the availability of water. Although its lumped behaviour is expected to be similar, spatial processes can result in a different behaviour and therefore other early warning signals than observed before (Dakos, 2008; Karssenberg & Bierkens, 2010). Spatial processes include the dispersion term in combination with the noise term[3] of equation 3, but also the redistribution of water discussed in next section.

3.1.2.3 Precipitation, infiltration and runoff generation

Water enters the system in the form of rain and leaves it via evapotranspiration and surface runoff. The frequency and intensity of the rain events within a year are modelled stochastically using a weekly timestep, while the duration of the events is fixed (one hour). Every week there is either one event or no event. This is determined by drawing a random number between 0 and 1. An event occurs if the random number is lower than the mean number of events per year (μ_{Freq}) divided by the number of weeks in a year (52). On average, the number of events per year will then sum up to μ_{Freq}.

If there is an event, the intensity [m/h] of this event is a random value drawn from a gamma distribution. Input parameters of the gamma probability density function are the shape and scale parameter (k and o respectively). The standard deviation and mean of the gamma distribution are: $\sigma_{Int}=k^{1/2}\cdot o$ and $\mu_{Int}=k\cdot o$, from which follows: $o=\sigma_{Int}^2/\mu_{Int}$ and $k=(\mu_{Int}/\sigma_{Int})^2$. Lowering the mean rainfall intensity while not altering its variance will change the shape of the probability density function as shown in appendix D.

Part of the rainwater infiltrates and recharges the soil column another part leaves the modelled area as runoff. The amount of water that infiltrates during an event is calculated using:

$$I_{event,i,j}=\min(I_{cap,i,j},\ p+q_{i-1,j}) \qquad (4)^4$$

$$q_{i,j}=p+q_{i-1,j}-I_{event,i,j} \qquad (5)$$

In these equations, $I_{event,i,j}$ is the amount of water that infiltrates during the event [m], $I_{cap,i,j}$ is the infiltration capacity [m/h], p is the rainfall intensity [m/h], $q_{i,j}$ is the discharge of water out of a cell [m/h].

Only as much as $I_{cap,i,j}$ can infiltrate (equation 4), the remainder is transported out of the cell (equation 5) into its neighbouring downstream cell. Using a while loop containing both equations, water is accumulated over the local drain direction map[5] (see accuthresholdfluxstate.m; based on: Karssenberg, 2006 and De Jong, 2009). In order to use this function, in which inflow is simply added to rainfall intensity, it should be assumed that ponding time is equal for all cells and all surface runoff leaves the modelled area during the rain event. This implies that infiltration down slope is not higher simply because it's ponded for a longer period.

Infiltration capacity ($I_{cap,i,j}$ in eq. 4) is usually strongly related to the vegetation cover. There are several reasons for this. First, soils covered by vegetation generally have a high macro porosity due to increased soil biological activity. In addition, the organic matter content is high under vegetation resulting in a well structured and permeable soil (Stroosnijder, 1996). A common process occurring on bare soils in arid regions is crust formation. Soils covered with crusts generally have a low hydraulic conductivity and therefore a low infiltration capacity (Stroosnijder, 1996). The cumulative result of these processes is simulated using one saturation equation:

---

[3] Note that the addition of noise is also needed to able to detect early warning signals. If there are no perturbations in the system, no signals related to critical slowing down can be observed.

[4] The infiltration ($I_{i,j}$ in equation 2) is the sum of $I_{event,i,j}$ over one year.

[5] Note that p=0 after the first iterative step and that the local drain directions are parallel (from top of the lattice to the bottom).

$$I_{cap} = I_{max} \frac{V + \gamma I_0}{V + \gamma} \qquad (6)$$

Equation 6 is a saturation function (see appendix B) that is also used in Rietkerk et al. (1997) to relate infiltration to biomass. In equation 6, I_{max} is the infiltration capacity at V=∞ [m/h], I_0 is the infiltration capacity of bare soil as a fraction of I_{max} [-] and γ is a saturation constant [kg/m²].

3.1.2.4 Spatial processes and scale

To determine the spatial scales to which WOTMOD can be applied, the (spatial) processes that are simulated should be evaluated. Two spatial processes were included in the model: dispersion of vegetation and the redistribution of water by runoff/runon processes. The size of the area modelled or grid cell size are not restricted by the dispersion of vegetation. One can just select a cell size and dispersion rate (D) that fit the area and properties of the vegetation that are modelled. The distribution of water by runoff/runon processes however, does limit the size of the area modelled. In section 3.1.2.3 it was assumed that all water leaves the modelled area within the duration of the rain event. This assumption is not valid if big areas are modelled. Another issue to keep in mind is the fact that some of the lumped processes discussed in the previous sections should be modelled spatially depending on the scale used. One could for example include an extra diffusion term to simulate the lateral flow of soil moisture (as in Rietkerk et al. 2002) for smaller scales, simulate the spatial grazing behaviour with greater detail or add some spatial variability to rain distribution if bigger areas are modelled. WOTMOD in its current form is expected to be valid for small areas ranging from hill slopes to small catchments.

3.1.2.5 Parameter values

The parameter values used in scenario 0 are listed in table 3.1. If other parameter values are used in other model runs, this will be indicated.

Table 3.1. Parameter values. Values marked with a * are initial values as they serve as drivers in scenario G, Freq or Int. See paragraph 4.2.

Parameter (script)	Symbol (text)	Value	Unit	Meaning
alpha	α	0.1	kg/m²	Half-saturation constant to relate grazing to vegetation density
beta	β	7	kg/m²	Saturation constant to relate evapotranspiration to vegetation density
c	c	18	kg/m³	Water use efficiency, biomass produced per volume of transpired water
d	d	0.5	y^{-1}	Maintenance rate
DV	D	0.2	y^{-1}	Dispersion rate of vegetation
Emax	E_{max}	2	m/y	Evapotranspiration at S=1 and V=∞
g	g	0.5*	kg/m²/y	Grazing rate
gamma	γ	0.75	kg/m²/y	Saturation constant to relate infiltration capacity to vegetation density
I0	I_0	0.3	-	I_{cap} as fraction of I_{max} at V=0
Imax	I_{max}	0.01	m/h	Infiltration capacity at V=∞
MeanFreq	μ_{Freq}	40*	events/y	Average number of rain events per year
MeanIntensity	μ_{Int}	0.01*	m/h	Mean rainfall intensity
por	n	0.4	-	Porosity
sdInt	σ_{Int}	0.0035	m/h	Standard deviation of the rainfall intensity
sdW	σ_W	1.5	kg/m²	Standard deviation of white noise on V
u	u	0.5	-	Determines the relationship between S and the

				evapotranspiration
V0	V_0	0.2	-	Evaporation as fraction of S^uE_{max} at V=0
Zr	Z_r	0.3	m	Depth of the rootzone
m, n	m, n	100, 100	cells	Number of cells in x and y direction

3.2 Scenarios

In the three main scenarios, three different drivers are used. In scenario G, grazing rate (g) is used to force a shift in the system. In scenario Freq, the mean number of rain events per year (μ_{Freq}) declines. The mean intensity of the rain events (μ_{Int}) decreases in scenario Int[6]. The outcome of these runs will be compared to reference scenario 0. For every run, the stochastic input (intensity and frequency of the rain events and white noise on vegetation density) is equal, so that the model output can be evaluated more easily. Based on the results obtained with the scenarios discussed above additional runs will be made to get more insight in the behaviour of the model under other parameter settings.

3.3 Analysis of model output

The analysis of the model output is guided by the generic early warning signals described in literature (section 2.2) and by the analysis of May's overharvesting model done in section 3.1.1 (figure 3.2). From this, changes in skewness, correlation and variance can be expected in space and time as well as flickering (bimodality in frequency distribution) between two stable states. The evaluation of the model on early warning signals is described below.

Every time step (year) a map (100x100 cells) of vegetation density and a map of annual discharge are generated by WOTMOD. These maps are analyzed by a separate script (analysis.m; appendix C.II.). For every map the spatial semivariance, range and sill of the semivariograms, lag-1,2,3 (cell lengths) spatial correlation, spatial variance and spatial skewness are calculated. The empirical semivariance is given by:

$$\gamma(h) = \frac{1}{2n(h)} \sum_{i=1}^{n(h)} (z(x+h) - z(x))^2 \qquad (7)$$

With:

$$h = \sqrt{h_x^2 + h_y^2}$$

In equation 7 (Bierkens, 2010), γ is the semivariance [m^2/y^2 or kg^2/m^4], h is the lag distance [cell lengths], h_x is the lag distance in x direction [cell lengths], h_y is the lag distance in y direction [cell lengths], n is the number of cell pairs that are considered [-] and z is annual discharge or vegetation density [m^2/y^2 or kg^2/m^4]. The script used to calculate the semivariance in x, y and xy direction can be found in appendix C.II.a. When plotting the semivariance against lag distance, a semivariogram can be obtained. By fitting a spherical model (using variogramfit.m by Schwanghart, 2009), two important properties of the semivariogram are derived: the sill [m^2/y^2 or kg^2/m^4] and the range [cell lengths]. The spatial correlation is for lag 1 to 3 cell lengths in x, y and xy direction are derived from the semivariance. Finally the spatial skewness and spatial variance are calculated for each map and histograms are made.

As early warning signals in timeseries are expected as well, 100 sampling cells were randomly selected[7]. For these cells, the vegetation density and annual discharge are stored every timestep, thereby creating 100 timeseries. For each of the timeseries the autocorrelation (for lag-1,2,3 y), skewness and variance are calculated using a moving window of 200 years (see skewtss.m, variancetss.m and corrtss.m in appendix C.II.c, C.II.d and C.II.e respectively). This way, changes over time can be observed. The outcomes for the 100 sampling locations are then averaged.

[6] Note that the variance in rainfall intensity remains constant. This affects the shape of the probability distribution of rainfall intensity (see appendix D).

[7] The sampling cells are the same for each model run.

4 Results

4.1 Model behaviour

4.1.1 A simplified version

Before the actual model was run, a simplified lumped version of the model was made to learn more about the behaviour of WOTMOD. This version only includes equation 2 and 3 and has no stochastic input. For different combinations of driver and initial values of V and S, this model ran till equilibrium was reached. Figure 4.1 was created by plotting these equilibrium values against driver[8], so each dot represents a stable system state for a certain value of the driver.

As shown in figure 4.1a, the equilibrium vegetation density left of the transition point decreases more or less linearly as grazing rate increases. A second stable state is situated at a much lower vegetation density. Soil saturation is rather insensitive to changes in vegetation density and therefore also not very sensitive with respect to grazing rate (see figure 4.1b). However, in the transition from a vegetated to a barren state, the soil saturation increases drastically[9]. A shift can also be caused by decreasing the infiltration (caused by changes in precipitation). A decrease in infiltration lowers the maximum growth rate and if grazing exceeds the maximum growth rate, this can result in a transition. Infiltration and equilibrium vegetation density are related in a similar (but mirrored) way as grazing rate and equilibrium vegetation density (figure 4.1c). However, equilibrium vegetation density seems to be much more sensitive to infiltration, even though they are not directly coupled in WOTMOD. Also note that the vegetation density at the last stable vegetated state is much lower than in figure 4.1a. In other words, the collapse of the system will be less pronounced when the infiltration (rainfall intensity/frequency) decreases than when the grazing rate increases. As shown in figure 4.1d, the jump in soil saturation will be smaller too. Soil saturation decreases to zero as infiltration goes to zero.

To find out how the model behaves under other parameter settings, a sensitivity analysis was done using an even more stripped version of the model. Now the grazing term of equation 3 is excluded and the soil saturation is assumed to be in equilibrium (dS/dt=0). The model runs once for each parameter setting from a vegetation density of close to 0 to the system's equilibrium. When, for the original parameter setting, vegetation growth is plotted against vegetation density, a bow-shaped curve (figure 4.2) similar to the growth curve in May's model (figure 3.1) can be found, with the difference that it is not symmetrical. Three interesting points in this graph are the maximum growth rate, the vegetation density at this maximum growth rate and the vegetation density at equilibrium (the same points were derived in appendix A for May's model). Under conditions without perturbations and small values of α, the transition takes place when the grazing rate exceeds the maximum growth rate. This is why the maximum growth rate can be considered as the grazing rate at transition (g_{crit}), and its corresponding vegetation density as the vegetation density at transition (V_{crit}). The vegetation density at the equilibrium (V_K) that is reached is comparable to the carrying capacity used in May's model. From these three points, two other important properties can be derived: the average slope in vegetation density till transition[10] (dV/dg; $(V_{crit}-V_K)/g_{crit}$) and the asymmetry of the growth curve (V_{crit}/V_K; 0.5 if symmetrical). The average slope in vegetation density till transition is an important property because when this slope is not very steep one would intuitively not expect sudden shifts in the system, as changing the grazing rate seems to have no significant effect on vegetation density. Table 4.1 shows how the system reacts to changes in parameter values. The sensitivity analysis shows that climate and/or soil properties (both linked to infiltration, I) as well as vegetation properties such as water use efficiency (c) and maintenance rate (d) affect the model output.

[8] Frequency and intensity of the rain events (used as drivers in respectively scenario Freq and Int) are represented by I, the infiltration.

[9] Note that infiltration is constant over the year and does not depend on vegetation density in this stripped version of the model. In WOTMOD the shift in soil saturation may therefore be less extreme.

[10] This slope can also be seen as the sensitivity of vegetation density to changes in grazing rate.

One interesting result of the sensitivity analysis is the fact that the growth curve (figure 4.2) shrinks in width and height when lowering the infiltration (so V_K, g_{crit} and V_{crit} decrease). This implies that if, due to changes in climate, the infiltration drops, the tolerance of the system to grazing decreases (g_{crit}). In the meantime, however, the collapse of the system would become less pronounced (V_{crit} is lower). In regions where vegetation has high water use efficiencies or low maintenance rates, the vegetation density at transition is high (V_{crit}). Grazing tolerance (g_{crit}) is low when the vegetation has high maintenance rates or low water use efficiencies. When maintenance rates or water use efficiencies are low, the sensitivity of vegetation density to grazing is low ((V_{crit}-V_K)/g_{crit}).

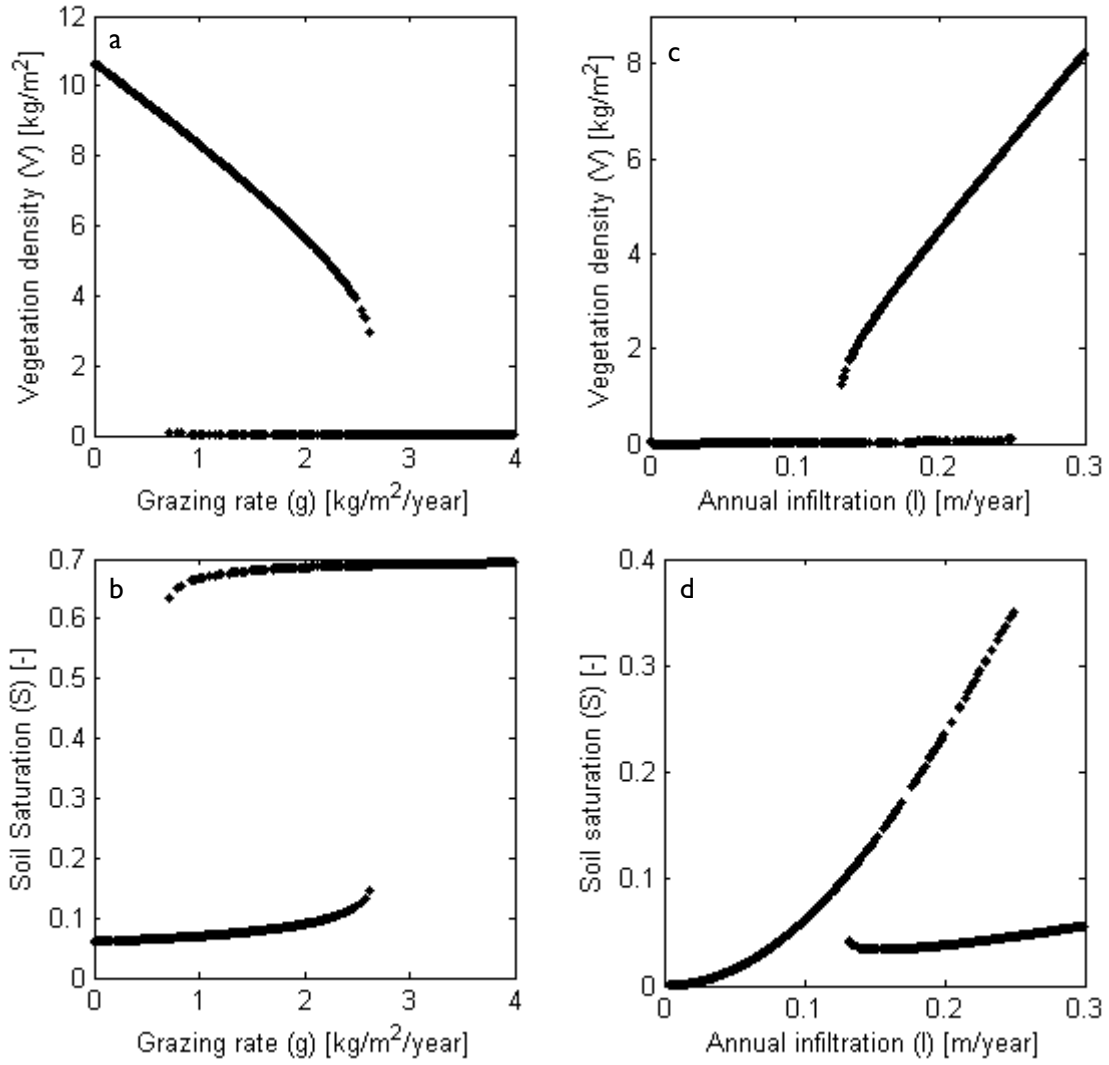

Figure 4.1. System state, vegetation density and soil saturation, against drivers.

Table 4.1. The effect of growth related parameters on model behaviour. Parameters are listed in order of sensitivity. Parameters between brackets have the same effect. See appendix E.1 for graphs of this sensitivity analysis and section 3.1.2 for explanation of the symbols.

	-	0	+
V_K	d, [V_0, β]	[Zr, n, u, E_{max}]	[I, c]
g_{crit}	[V_0, d, β]	[Zr, n, u, E_{max}]	[I, c]
V_{crit}	d	[Zr, n, u, E_{max}]	[I, c], [V_0, β]
V_{crit}/V_K	[I, c]	[Zr, n, u, E_{max}]	[V_0, d, β]
(V_{crit}-V_K)/g_{crit}	[V_0, β]	[Zr, n, u, E_{max}]	d, [I, c]

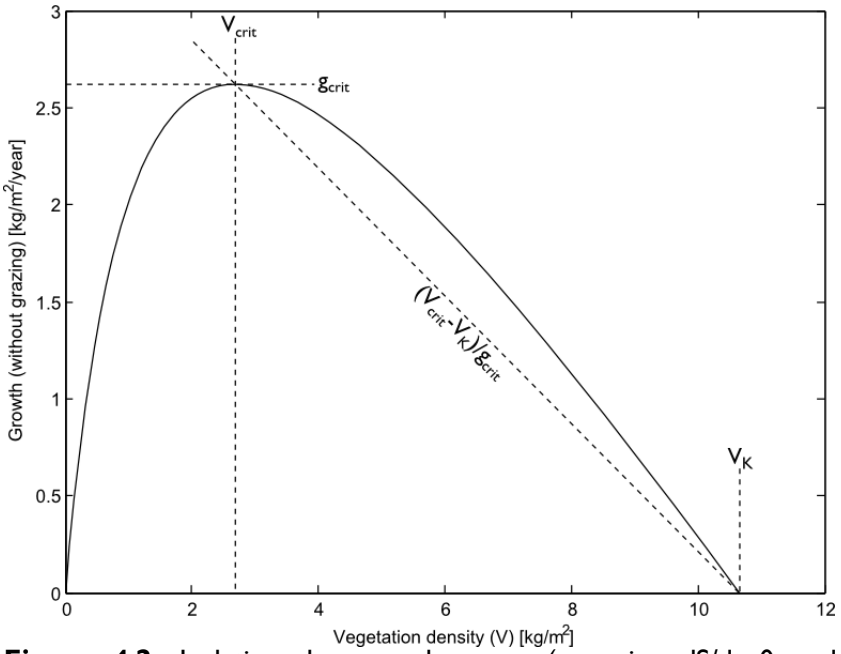

Figure 4.2. Isolating the growth curve (assuming dS/dt=0 and I=0.335 m/y) in WOTMOD results in a bow shaped curve.

4.1.2 Scenarios

4.1.2.1 Scenario G

Increasing the grazing rate from g=0.5 kg/m²/y in year 200 to g=2.5 kg/m²/y in year 2200 (0.2% of initial g per year), results in a shift in vegetation density in year 1875 as shown in figure 4.3. The perturbations are caused by the noise that is added to the vegetation density and indirectly by the stochastically modelled rainfall frequency and intensity. The shift occurs at a lower grazing rate (2.2 kg/m²/y) than predicted by the simplified version of the model of section 4.1.1 (2.6 kg/m²/y), for which it was assumed that infiltration is not related to vegetation density and that was not subject to stochastic input. The shift is also visible in total annual discharge (figure 4.4), although discharge seems to be rather insensitive to vegetation density before transition, as no clear trend can be observed.

Figure 4.5 shows that no clear spatial patterns in vegetation density can be observed before the transition (no vegetation patches or accumulation of vegetation in downstream regions). Close to the transition point, small gaps in vegetation cover emerge and slowly expand. During transition, vegetation patches form for a very short period. This can also be seen in a graph of map averaged vegetation density (appendix E.I; figure E6), in which the transition seems to be paused for a while. To see whether these spatial patterns are created by the redistribution of water caused by the runoff/runon processes described in section 3.1.2.3, an extra model run was. For this run the generation of runoff was "switched off", so that the excess of water was not transported to downstream cells and no infiltration of runon could occur. In this run, no patches formed.

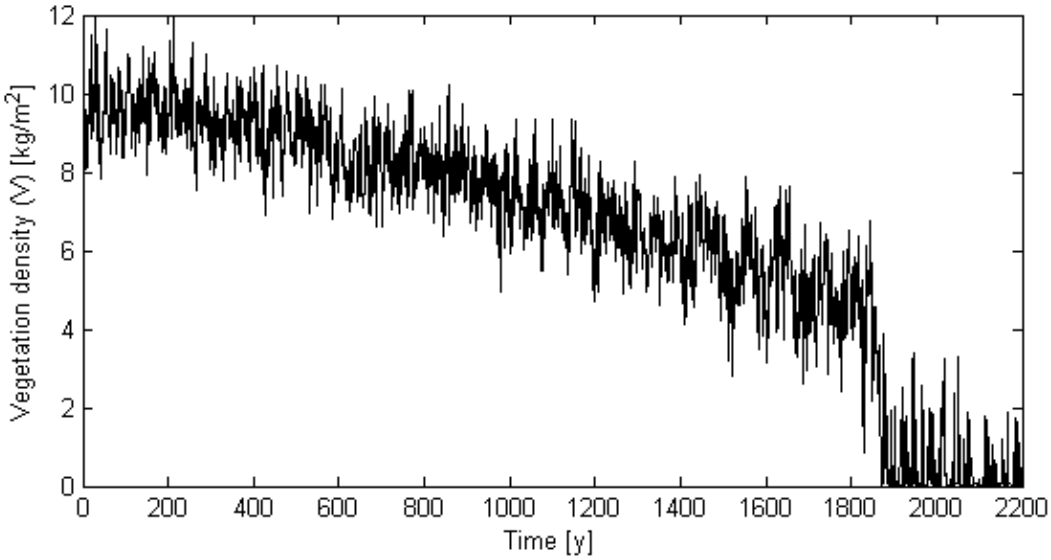

Figure 4.3. Vegetation density against time at [50, 50]. See appendix E.I, figure E6 for the map averaged vegetation density over time and figure E7 for a plot of vegetation densities at the sample points.

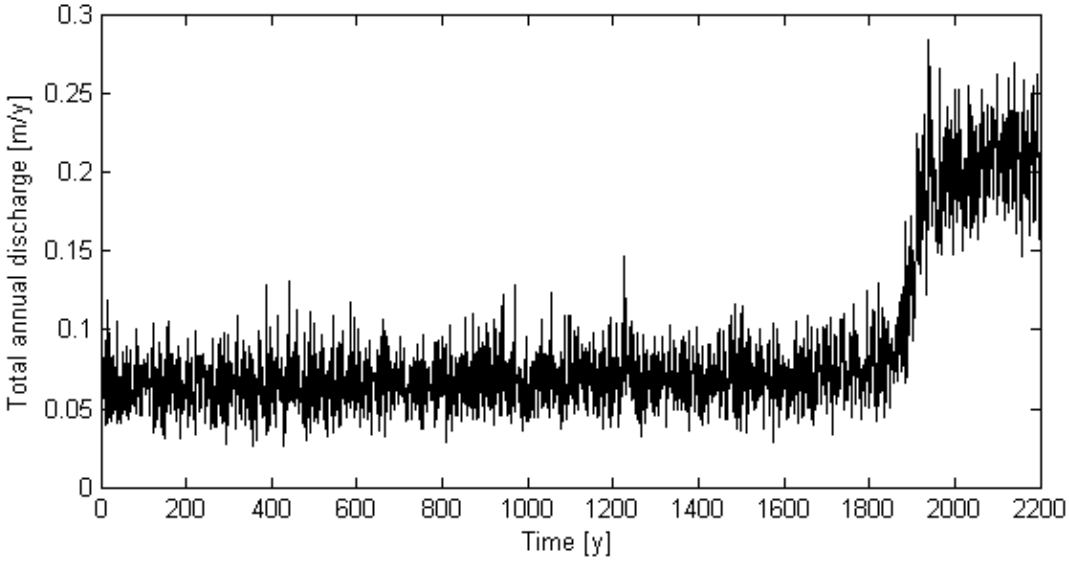

Figure 4.4. Total annual discharge [m/y] against time.

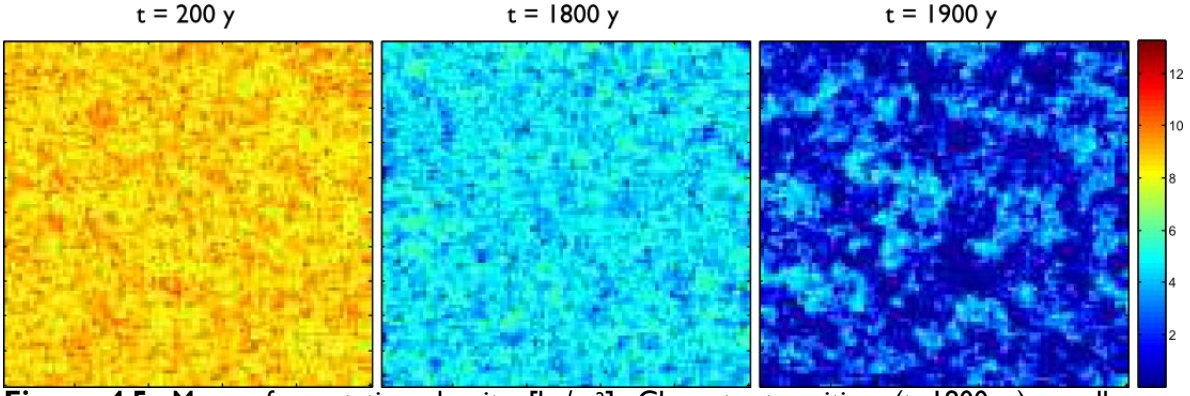

Figure 4.5. Maps of vegetation density [kg/m²]. Close to transition (t=1800 y), small gaps in vegetation cover appear and expand. Vegetation patches (t=1900 y) are stable for about 30 years. A vegetation density map at t=1900 y with a scaled legend can be found in appendix E.I, figure E8.

4.1.2.2 Scenario Freq and Int

Since the system state is more sensitive to precipitation than to grazing, the frequency and intensity of the rain events were lowered with respectively 0.03% and 0.035%[11] of their original values per year. Figure 4.6 shows that this does not result in the expected transition. In both scenarios, the vegetation density declines more or less linearly over time. A transition can be observed if α is lowered. The total annual discharge from the modelled area decreases in scenario Int (see appendix E.I., figure E9). In scenario Freq no clear trend in discharge can be observed (figure E10), as a decrease in vegetation density leads to a lower infiltration capacity and therefore more runoff, counteracting the decrease in annual precipitation. No vegetation patches form in these two scenarios.

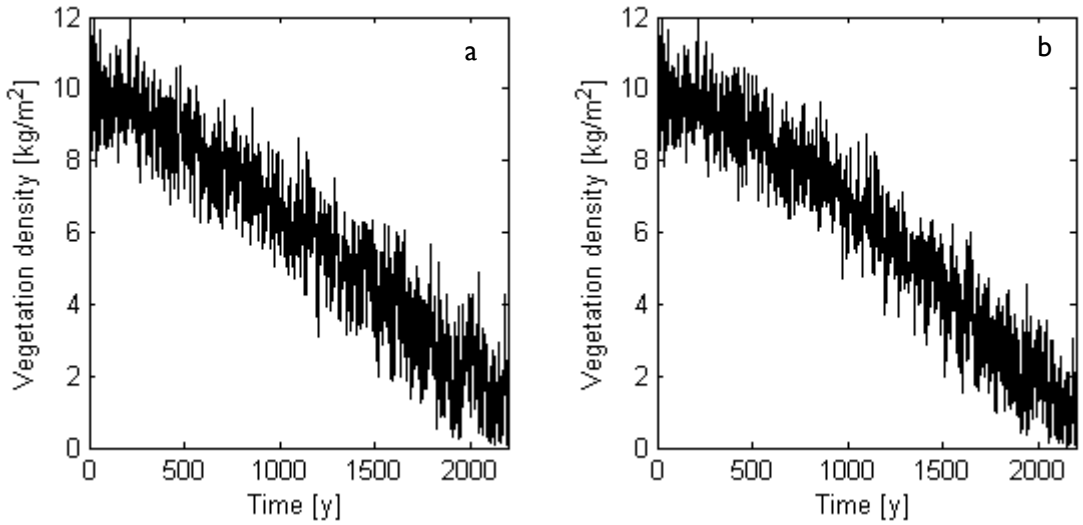

Figure 4.6. Vegetation density at [50, 50] over time for scenario Freq (a) and Int (b).

4.2 Early warning signals

4.2.1 Scenario G

Before the transition in scenario G, early warning signals in vegetation density can be detected. The signals appear both in time and space.

Over time, the averaged autocorrelation in vegetation densities measured at the 100 sample points increases (figure 4.7a). The averaged variance in vegetation density at the sample points increases as well (figure 4.7b) and the skewness declines (figure 4.7c). Although the trends are clear, it should be noted that, for example the skewness in vegetation density in scenario G incidentally exceeds the skewness in scenario 0, while the stochastic input is equal for both scenarios. This means that a higher grazing rate does not necessarily result in a lower skewness in vegetation density. The same holds for variance and autocorrelation.

Spatial signals in vegetation density can be found as well. Before the transition, the spatial correlation increases (figure 4.8a), the variance increases (figure 4.8b) and the skewness declines (figure 4.8c). Spatial correlation parallel and perpendicular to stream direction are equal and so are the semivariograms. The sill of the semivariograms (figure 4.8e-f) is equal to the variance and therefore it increases over time. The range increases too (figure 4.8d).

No clear early warning signals can be found in annual discharge. An example is given in appendix E.II. Figure E11 shows that before the transition, the autocorrelation in annual discharge for scenario 0 and G are almost equal. During the transition, the autocorrelation is higher in scenario G (figure E12), but this can obviously not be considered as an early warning signal for the transition.

[11] The decrease in rainfall intensity is greater than the decrease in frequency, as less precipitation will be lost as runoff if the intensity decreases, so a larger proportion infiltrates.

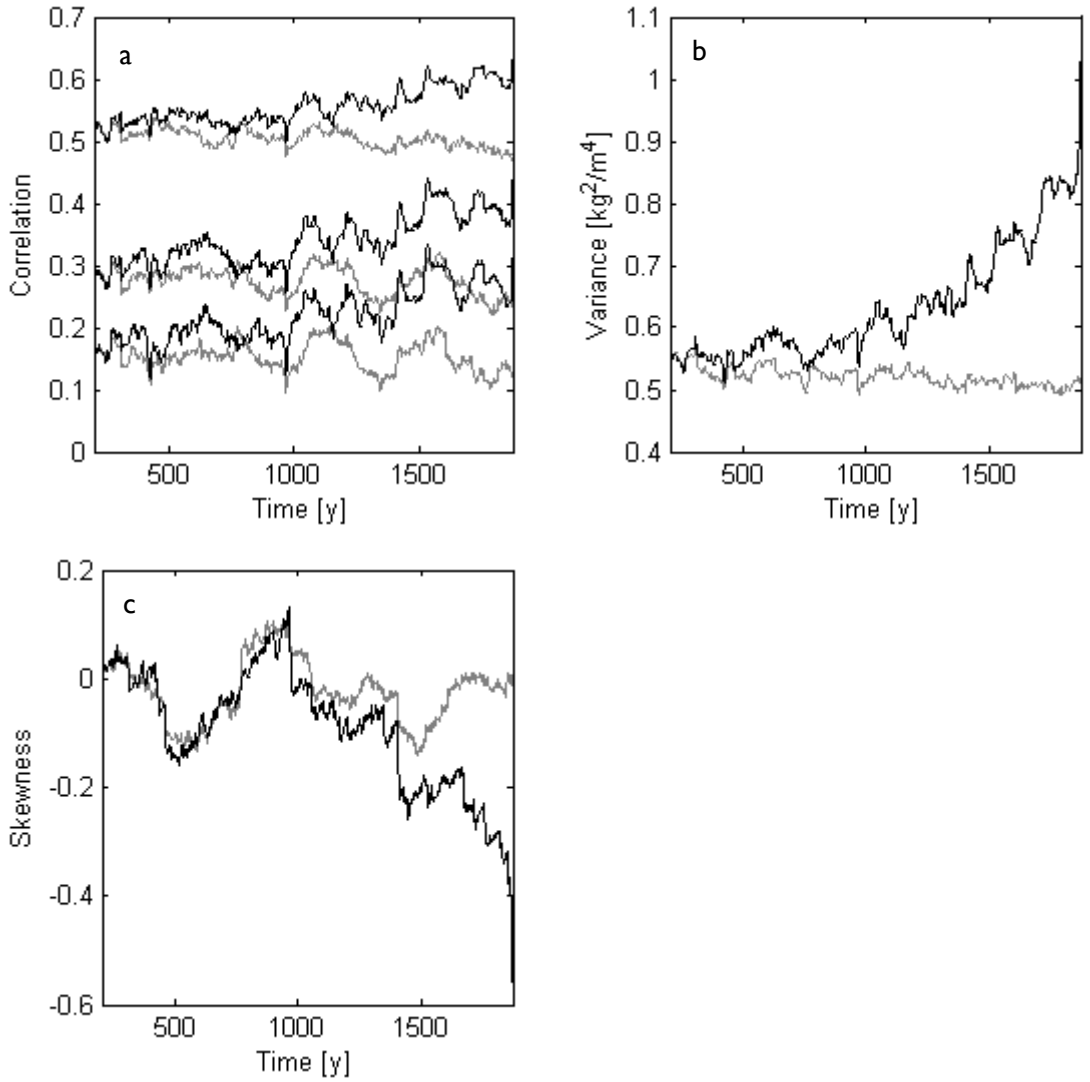

Figure 4.7. Early warning signals in time series data of vegetation density at sample points. Figures were made using a moving window of 200 years and by averaging the obtained values for the 100 sample points. a) Autocorrelation for h=1, 2 and 3 year, b) temporal variance and c) temporal skewness. In black: scenario G. In grey: scenario 0.

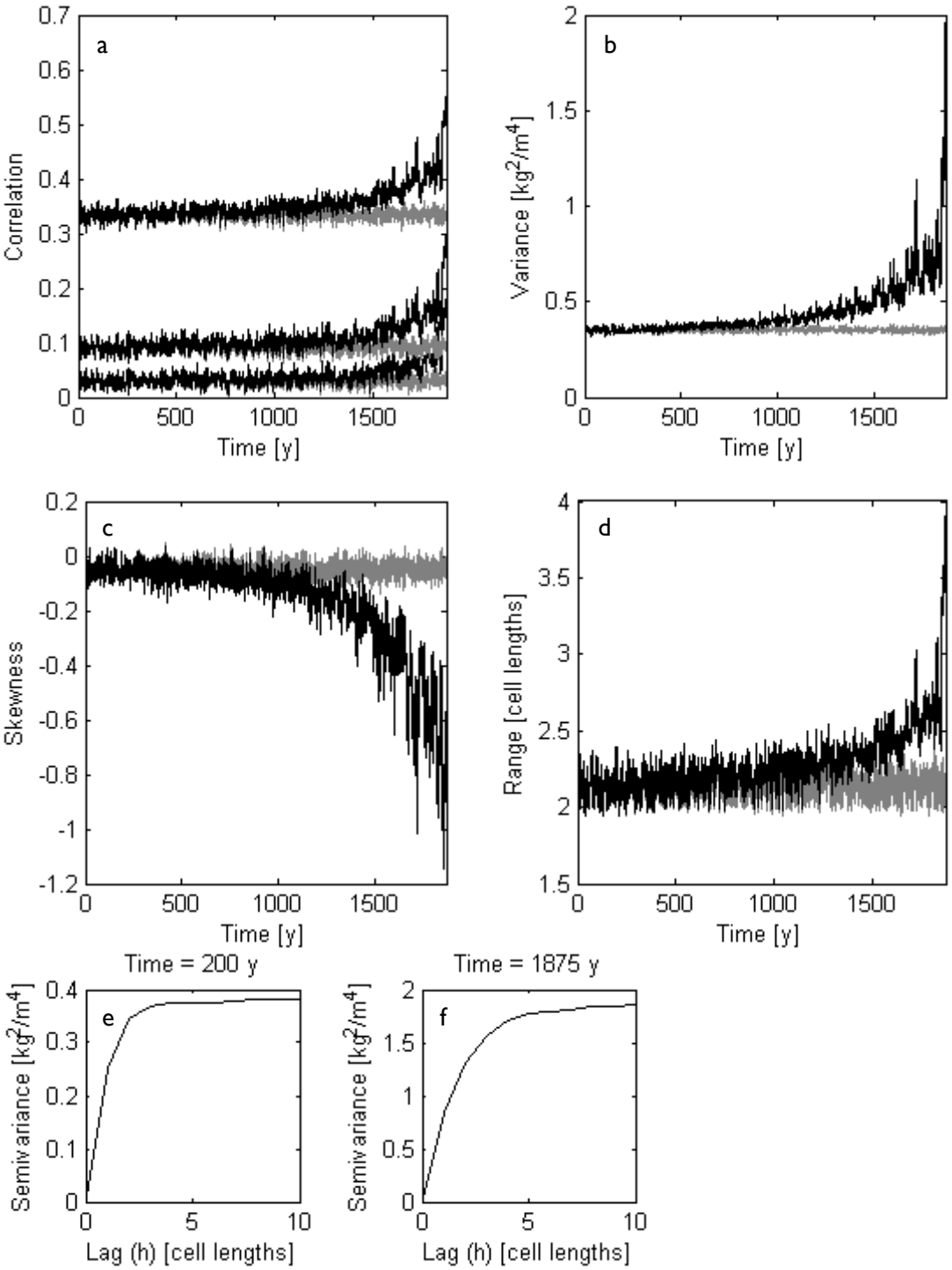

Figure 4.8. Early warning signals in vegetation density maps. a) Spatial correlation over time for h=1,2 and 3 cell lengths, b) spatial variance, c) spatial skewness, d) range of semivariograms of vegetation density maps, e) emperical semivariogram at t=200 y, f) empirical semivariogram at t=1875. In black: scenario G, in grey: scenario 0.

4.2.2 Scenario Freq and Int

Although no critical transition takes place in scenario Freq and Int, early warning signals can be observed in vegetation density. Especially in variance and correlation over time and space clear signals can be detected (see appendix E.II; figures E13 and E14). These signals have a similar strength as in scenario G, but the trend in temporal and spatial skewness seem to be much weaker. Another difference is that, during the transition in scenario G, the correlation and variance increase and the skewness decreases drastically (e.g. figure E12). This is not the case in scenario Freq and Int.

4.3 Additional runs

From the results so far, the question arises how the model behaves under other parameter settings. For example, how does the formation of vegetation patches, found in scenario G, depend on the relation between vegetation density and infiltration capacity? And can signals in annual discharge be found if the generation of runoff is more sensitive to vegetation density? These questions will be answered in this section.

4.3.1 Lower I_0

From the model study by Rietkerk et al. (2002) it can be concluded that the self-organisation of vegetation in patches depends on the difference in infiltration rate between vegetated and bare soil. The function that relates infiltration rate to vegetation density in Rietkerk's model is similar to what is used in WOTMOD to relate infiltration capacity to vegetation density (equation 6). By lowering I_0, the difference in infiltration capacity for vegetated and non vegetated soils can be increased. It is expected that this will result in a more stable patchy state and more pronounced self-organisation of vegetation than in scenario G. The value of I_0 was changed from 0.3 to 0.05 and grazing rate is used as driver. The results are presented below.

As expected, more stable patches form and sustain for a longer period (about 200 y). Now, clearly two shifts can be observed: one from a fully vegetated state to a patched state and the other from a patched state to a barren state (figure 4.9). The first shift takes place at t=1675 y, so sooner than in scenario G (t=1875). This is caused by the fact that lowering I_0 also leads to a decrease in infiltration at vegetation densities higher than zero, thereby decreasing the tolerance to grazing. If the spatial redistribution of water is excluded from the model (the generation of runoff is "switched off"), no vegetation patches form (see appendix E.II., figure E15). During the patched state, the semivariograms perpendicular and parallel to the flow direction clearly differ. Perpendicular to the slope, the semivariance increases with lag distance till the sill is reached, just like in scenario G. Parallel to the slope however, oscillating behaviour in semivariance can be observed. Figure 4.10b, shows that cells that are 25 to 40 cell lengths apart from each other are more correlated than cells separated by 10 to 25 cell lengths. Just like modelled by Rietkerk et al. (2002), the vegetation bands slowly move uphill.

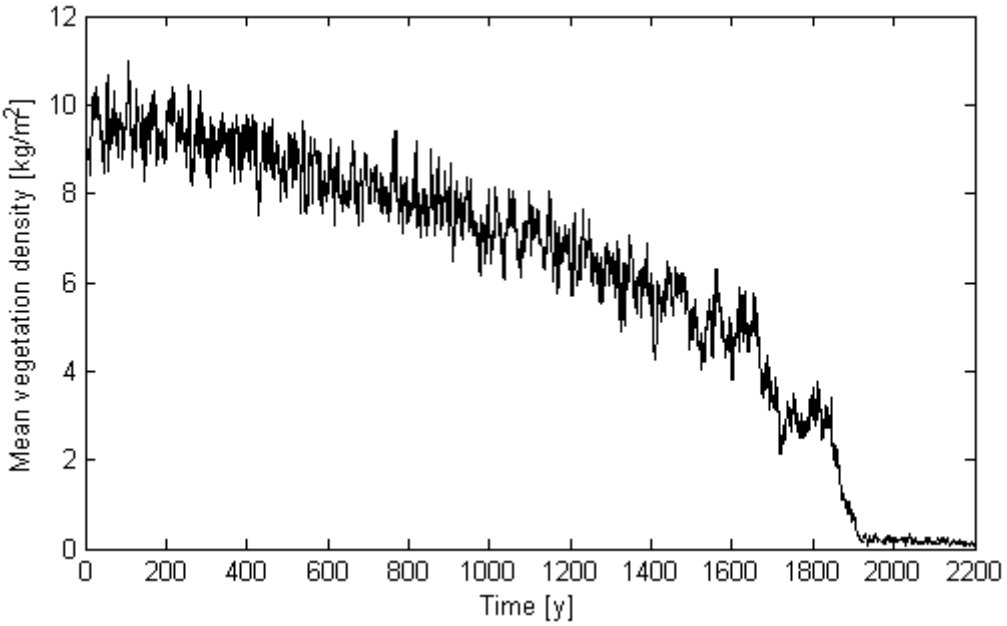

Figure 4.9. Map averaged vegetation density over time. In this model run clearly three system states can be distinguished: a fully vegetated state (t=1-1675 y), a patchy state (t=1676-1875 y) and a barren state (t=1876-2200).

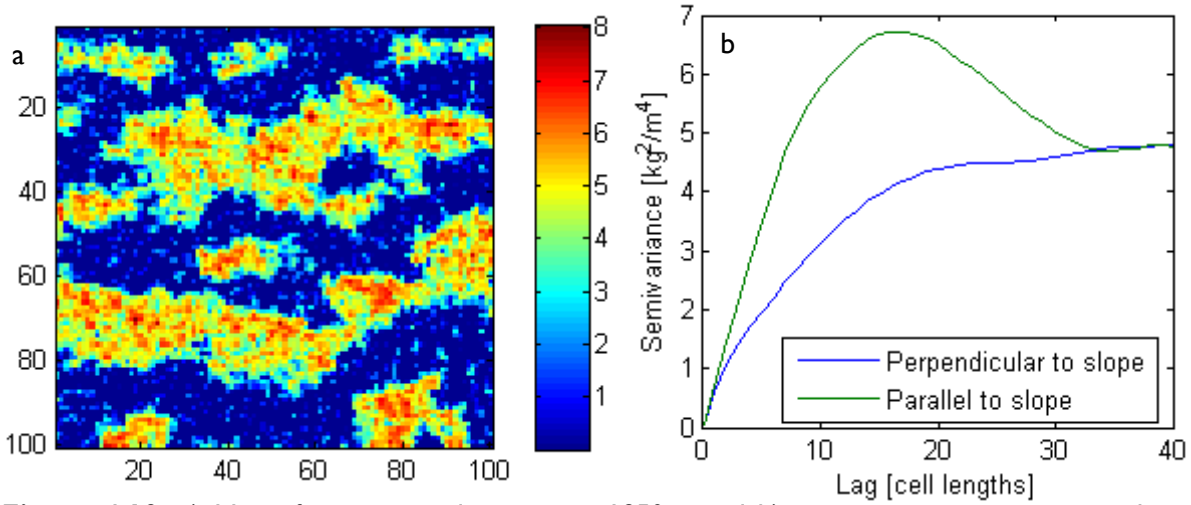

Figure 4.10. a) Map of vegetation density at t=1850 y and b) semivariance in vegetation density perpendicular and parallel to the slope at t=1850 y.

4.3.2 Higher sensitivity of I_{cap} at $V>V_{crit}$

In scenario G, no early warning signals were found in annual discharge. Annual discharge is linked to vegetation density via the saturation function that relates infiltration capacity to vegetation density (equation 6). A decrease in V leads to a decrease in I_{cap} and thereby to an increase in runoff. However, at high vegetation densities, so before the transition, I_{cap} is rather insensitive to changes in V (figure 4.11). This insensitivity could be the reason for the fact that no signals were found in annual discharge in scenario G, as the signals present in vegetation density could not be transferred to the generation of runoff. Increasing the slope of the saturation function of equation 6 at high vegetation densities could result in clearer early warning signals in annual discharge. In this additional run, I_{max} and γ were increased to 0.013 m/h and 5.25 kg/m² respectively. To keep the infiltration capacity of bare soil ($I_0 I_{max}$) equal, I_0 was lowered to 0.23.

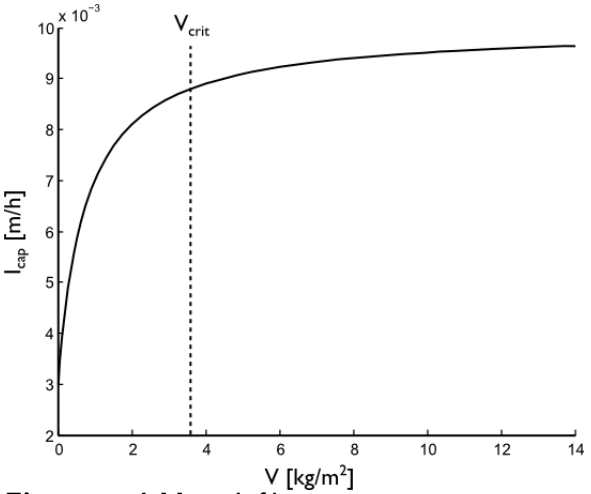

Figure 4.11. Infiltration capacity against vegetation density (equation 6). Before transition, infiltration capacity is not very sensitive to vegetation density. V_{crit}: vegetation density at transition.

Increasing the sensitivity of I_{cap} to V resulted in a transition at t=1300 y. As shown in figure 4.12b, a much clearer trend in annual discharge till transition can be observed compared to scenario G (figure 4.4). Also trends in autocorrelation and temporal variance can be observed in annual discharge, while there is no clear change in temporal skewness (figure 4.12b-d). Note that the increase in variance, may also be caused by the fact that the mean annual discharge increases over time.

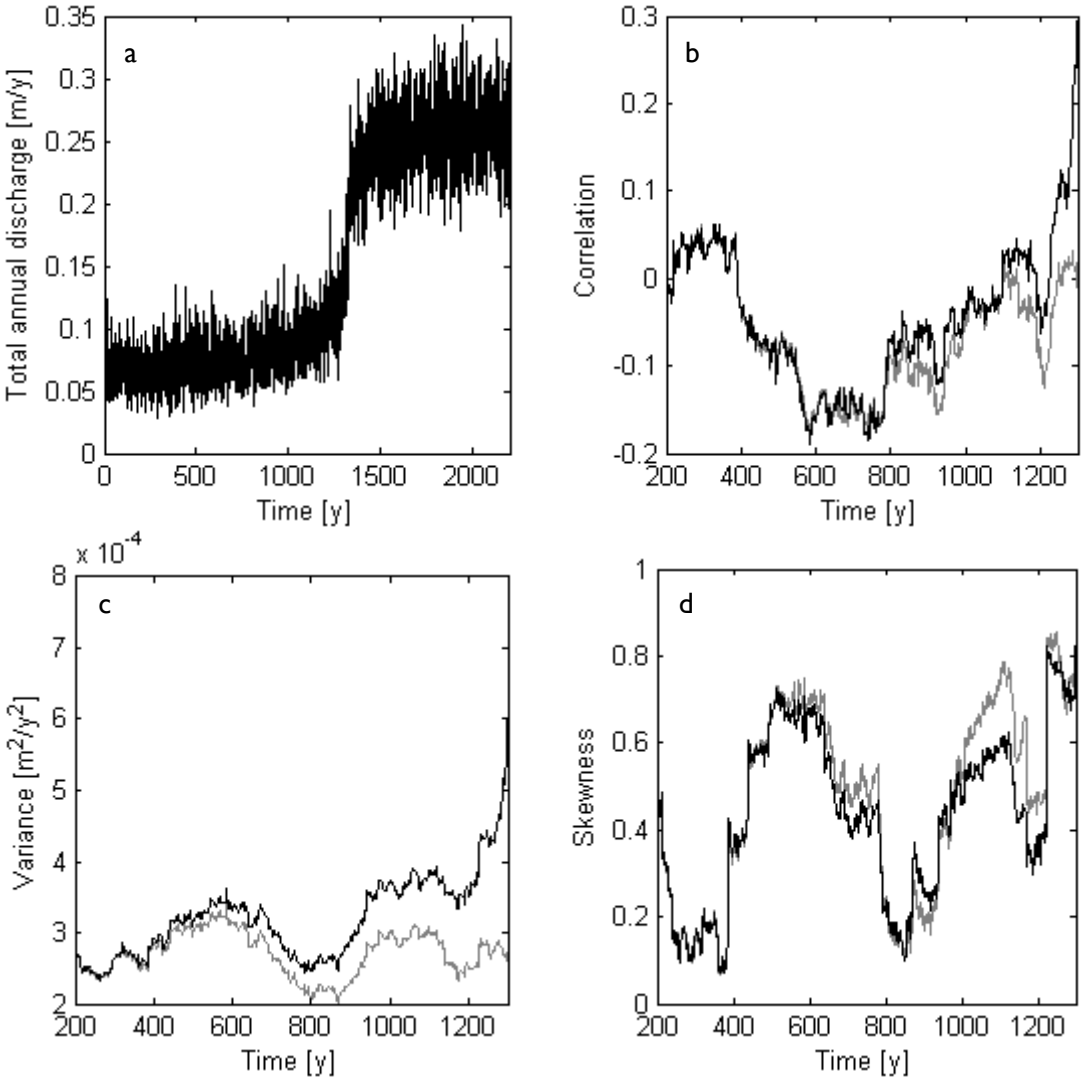

Figure 4.12.[12] a) Total annual discharge over time, b) lag-1-autocorrelation over time, c) temporal variance and d) temporal skewness. Grey: scenario 0, black: scenario G. Both scenarios with: I_{max} = 0.013 m/h, γ=5.25 kg/m^2 and I_0=0.23.

[12] Only indicators in time serie data from the sample points are shown as measuring spatial distribution of annual discharge is not possible in practice.

5 Discussion

WOTMOD contains two types of mechanisms that can result in a transition, refered to as grazing and resource feedbacks in section 2.3. The grazing feedback mechanisms in WOTMOD were broadly discussed in section 3.1.1. The resource feedbacks were modelled before by Rietkerk et al. (2002). From the results it can be concluded that depending on the parameter setting or driver used, either both (scenario G with low I_0), none (scenario Freq and Int) or one (scenario G) of these mechanisms can result in a transition. For both transitions early warning signals appear.

5.1 Grazing feedback mechanisms and early warning signals

The grazing feedback mechanisms, responsible for the main (lumped) transition in WOTMOD, were discussed in section 3.1.1. However the system did not behave as expected. Decreasing the infiltration of water into the rootzone by altering the intensity or frequency of the rain events was expected to cause a shift in vegetation density, as the maximum growth rate was expected to drop below the grazing curve (figure 5.1a). This however is not what happened in scenario Int and Freq. Decreasing the infiltration does not only result in a lower maximum growth, but also in a drop in vegetation density at this maximum and a lower carrying capacity (see table 4.1). In other words, the growth curve as a whole shrinks. This allows the growth curve to move to the left side of the grazing curve, so that no transition can take place (figure 5.1b). Under other parameter settings (lower alpha) a transition can be forced using rainfall frequency or intensity. This leads to the conclusion that transitions based on grazing feedback mechanisms are less likely to occur due to changes in precipitation.

The absence of the transitions in scenario Freq and Int was not predicted by the simplified model of section 4.1.1. In this model it was assumed that infiltration capacity is independent of vegetation density. This is however not how it was modelled in WOTMOD. At low vegetation densities in WOTMOD, the infiltration capacity increases with vegetation density resulting in a steeper left side of the growth curve of figure 4.2. A steep left side of the growth curve makes the occurrence of a transition less likely, especially when the infiltration declines, since this moves the growth curve to the left.

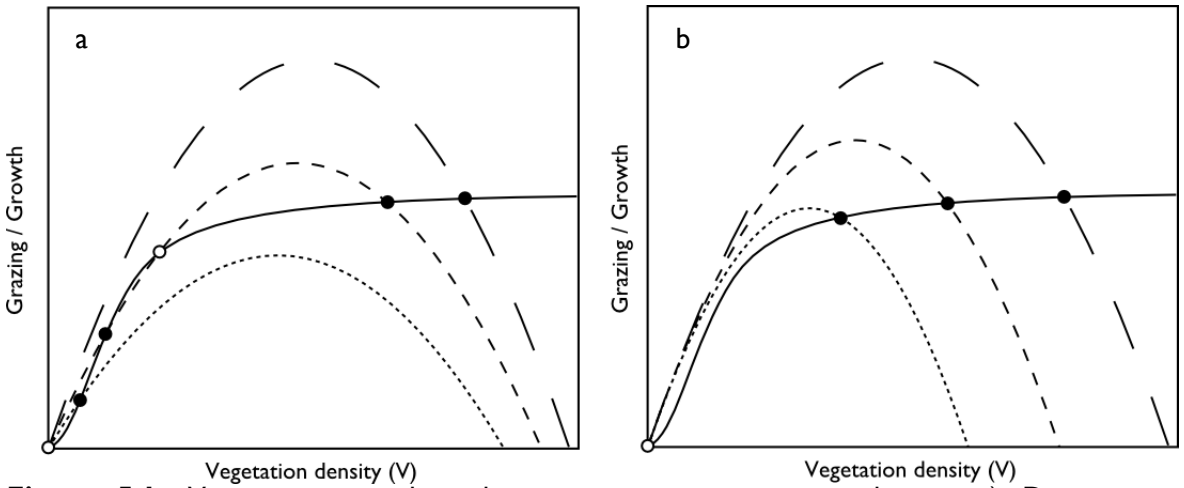

Figure 5.1. Vegetation growth and grazing against vegetation density. a) Decreasing the frequency/intensity of the rain events results in a transition (expected) and b) decreasing the frequency/intensity of the rain events does not result in a transition (scenario Freq and Int). Solid dot: stable equilibrium, open dot: unstable equilibrium, solid line: grazing and dashed lines: vegetation growth (infiltration decreases with dash size).

For the transition based on grazing feedback mechanisms, early warning signals were detected in map- and time series data of vegetation density and annual discharge. These signals were found in temporal and spatial correlation, variance and skewness. Although the trends in these

measures are clear, more pronounced trends were found in other model studies, including studies that used a spatial version of May's model (Dakos, 2009; Karssenberg & Bierkens, 2010). The reason for this is thought to be the fact that noise is added to the system via both the noise on the vegetation density maps and the stochastically modelled rainfall frequency and intensity. The noise on vegetation density does not affect the system as a whole, as it is normally distributed around zero, so the net effect on the map of m·n cells is close to zero. In contrast, the noise added via the variability in precipitation does affect the state of the whole system, as it determines the infiltration for all cells on the map. A dry year pushes the system closer to the transition while a wet year does the opposite. This results in extra noise in correlation, variance and skewness, and therefore weaker trends. This makes it unlikely that early warning signals will be found in reality as many sources of noise are present in real systems, such as variability in grazing rate.

The trends in variance and spatial-/autocorrelation that were detected are caused by a decreasing recovery rate. Figure F1 in appendix F shows the correlation between annual precipitation and map averaged vegetation density. Over time the correlation decreases, so the state of the system becomes less correlated to the noise that is added. This implies that not only the recovery rate declines when approaching the transition, but also the response rate. A decrease in response rate can in theory result in a decrease in variance over time (Scheffer, 2009) instead of an increase which was found in this study.

It is remarkable that trends in variance and correlation can be found even though no shift takes place in scenario Freq and Int. This leads to the conclusion that increasing variance and correlation cannot be used as early warning signals for (critical) transitions when considering this system. In contrast, the increase in skewness was much less in scenario Freq and Int compared to scenario G. Another difference between scenario G and Freq/Int is that during the transition in scenario G, extreme increases in variance and correlation and drops in skewness can be detected. These fluctuations however cannot be considered as early warning signals as they occur during and not before the transition.

Early warning signals in discharge seem to depend on the relation between vegetation density and infiltration capacity. If infiltration capacity is insensitive to vegetation density before the transition, no signals will appear in discharge. If infiltration capacity is more sensitive to vegetation density, signals appear in temporal variance and somewhat weaker in autocorrelation. This implies that signals are transferred from vegetation density to annual discharge via infiltration capacity. It is not clear why no signals appear in temporal skewness.

5.1.2 Resource feedback mechanisms and early warning signals

The vegetation patches that form for a short period in scenario G and in the additional run with a lower I_0 are the result of feedback mechanisms within the water-vegetation subsystem, referred to as resource feedback mechanisms before. The formation of vegetation patches is the cause of the second transition in scenario G with low I_0, but in the meantime these patches serve as an early warning signal for the transition.

The self-organisation of vegetation in patches or bands can be seen as a survival mechanism as it generally leads to higher average vegetation densities compared to the homogeneous situation (Rietkerk et al., 2002). The formation of vegetation patches is thought to be caused by the fact that facilitative and competitive interactions between plants operate at different spatial scales (Couteron & Lejeune, 2001). In WOTMOD, growth is limited by water and infiltration capacity is controlled by vegetation density. At high vegetation densities more water can infiltrate, which is a facilitating feedback mechanism that operates at a local scale. However, surface water that infiltrates upsteam cannot infiltrate downstream, so competitive interactions act at a larger spatial scale. Within a vegetation band the surface water is depleted, so that at downstream side of the band growth is limited. On bare soil almost no water infiltrates which prevents vegetation to grow, but also causes surface water to accumulate. This surplus of water is transported in downstream direction to the next vegetation band. This is what forms and maintains the vegetation bands.

The results can partly be explained by what is described in literature about self-organisation of vegetation in arid regions. For example, lowering I_0 resulted in a more pronounced and more

stable patched state which is consistent with what was found by Rietkerk et al. (2002). Some of the results however, cannot be explained by other studies. It is for example not clear why vegetation patches form in scenario G and not in scenario Freq and Int, while the same parameter settings are use.

Figure 5.2 shows the infiltration capacity against vegetation density. On x-axis the minimum and maximum value of V on a map for a specific time are marked. On the right side of this figure, the probability distribution of the rainfall intensity used in scenario 0, G and Freq is plotted. As shown, three types of rain events can be distinguished. Events of type 1 have an intensity higher than the highest infiltration capacity on the map, with the result that runoff is generated on all cells on the map. However, no infiltration of runon occurs as for all cells infiltration capacity is already reached. Events of type 1 do not result in patch formation since no spatial competition for water takes place. These events can however have an amplifying effect on the variance in vegetation density: cells with high vegetation densities have higher infiltration capacities, causing more water to infiltrate and consequently an increase in growth. In contrast to type 1 events, there are events of type 3 which have a homogenizing effect. Type 3 events have an intensity lower than the lowest infiltration capacity, so no runoff is generated and for all cells an equal amount of water infiltrates. Since there is no spatial redistribution of water, no spatial competition occurs. Type 2 events are rain events with an intensity higher than the minimum and lower than the maximum infiltration capacity on the map. These events trigger the formation of vegetation patches as both runoff generation and runon infiltration occur[13], which allows spatial competition to take place.

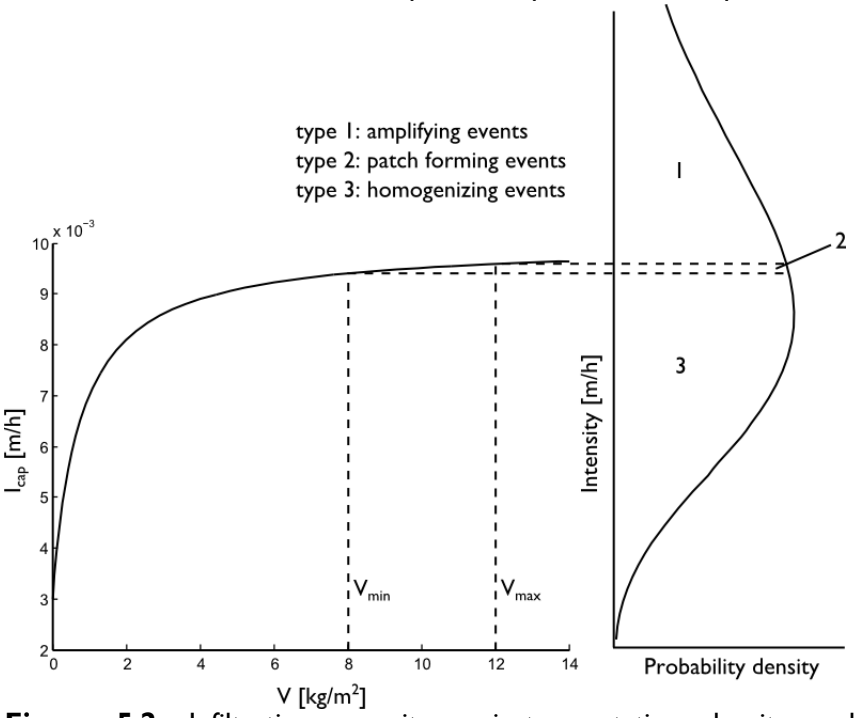

Figure 5.2. Infiltration capacity against vegetation density and probability distribution of the rainfall intensity. Three types of rain events can be distinguished. Events with a high intensity (1) have an amplifying effect on variance in vegetation density while events with a low intensity (3) have a homogenizing effect. Only events with an intermediate intensity (2) trigger patch formation.

When the variance in vegetation density is larger, the occurrence of patch forming rain events (type 2) is more likely (see figure 5.2). When the vegetation density is lowered, due to increased grazing or decreased annual precipitation, the probability of patch forming rain events to occur becomes either higher or lower. This depends on the relation between V and I_{cap} and on the

[13] Only if cells on which runoff is generated (I_{cap}<Int) are located upstream of cells for which the infiltration capacity is not yet reached (I_{cap}>Int).

shape of the probability density function that is used, since the probability that a type 2 event occurs is represented by the area under the probability density curve.

From this analysis of patch formation in WOTMOD it is hypothesized that self-organization in semi-arid ecosystems does not only depend on the relationship between vegetation density and infiltration but also on the probability distribution of rainfall intensity and the variance in vegetation density. If this hypothesis is valid, this would imply that not only soil and vegetation properties – such as the difference in infiltration rate on vegetated and bare soils found by Rietkerk et al. (2002) – determine the formation of vegetation patches but also (the variability of) the climate. It would also explain the results obtained in this study. In contrast to scenario G, no vegetation patches formed in scenario Freq and Int. For scenario Int this could partly be caused by the fact that more homogenizing (type 3) rain events occur when the intensity declines. This is however not the case in scenario Freq. The absence of vegetation patches in scenario Freq could be due to the fact that no transition based on grazing feedback mechanisms takes place. In scenario G the transition caused a big increase in variance during the transition, which allowed more patch forming (type 2) events to occur. This implies that patch formation can be triggered by other transitions, like the one modelled in WOTMOD.

To test the hypothesis further research is needed. It is advised to exclude the lumped transition in WOTMOD, caused by grazing feedbacks, as this will result in a better understanding on the patch forming processes. This can, for example, be done by assuming that grazing increases linearly with vegetation density.

6 Conclusion

In water-controlled ecosystems subject to grazing two types of transitions can occur. One is related to feedbacks between grazing and vegetation growth, the other is caused by feedbacks between vegetation and its limiting resource: water.

For transitions caused by the first feedback mechanism early warning signals related to critical slowing down – increasing correlation and variance – as well as changes in skewness can be detected in vegetation density in space and over time. Depending on the relation between vegetation density and infiltration capacity, increasing variance and autocorrelation can be found in annual discharge. If no critical transition occurs, these signals can still be observed. Declining rainfall intensity or frequency are less likely to trigger a critical transition that is related to grazing feedbacks. Trends in skewness, variance and correlation can be weakened by the variability of the climate.

Transitions caused by feedbacks between water and vegetation, early warning signals appear in the form of vegetation bands. It is hypothesized that the formation of these vegetation patterns does not only depend on the relationship between vegetation density and infiltration but also on the probability distribution of rainfall intensity and the variance in vegetation density.

Acknowledgments

I would like to thank Derek Karssenberg for the overall supervision of the project and Marc Bierkens and Max Rietkerk for giving the information I needed during model development. I want to thank Maarten Zeylmans for giving me access to the fast computers in the GIS-room on the fourth floor of the van Unnik building and the staff of the Earth sciences and the Environmental sciences programmes for sharing their knowledge with me over the past four and a half years. Finally, I would like to thank my fellow students for their support and their useful input during the project.

References

Bierkens, 2010. Stochastic Hydrology, GEO4-4420. Department of Physical Geography. Utrecht University.

Boer, de, R.J., 2010. Modeling Population Dynamics: a Graphical Approach. Theoretical Biology & Bioinformatics. Utrecht University. Available on http://theory.bio.uu.nl/rdb/books/.

Couteron, P., and O. Lejeune, 2001. Periodic spotted patterns in semi-arid vegetation explained by a propagation-inhibition model. Journal of Ecology 89, 616-628.

Dakos, V., E.H. van Nes, Raúl Donangelo, Hugo Fort and Marten Scheffer, 2009. Spatial correlation as leading indicator of catastrophic shifts. Theoretical Ecology 3(3), 163-174.

Daly, E., A. Porporato and I. Rodriquez-Iturbe, 2004. Coupled Dynamics of Photosynthesis, Transpiration and Soil Water Balance. Part 1: Upscaling from Hourly to Daily Level. Journal of Hydrometeorology 5, 546-558.

Dekker, S.C. and M.B. Eppinga, 2007. Milieusysteemanalyse en Modellen, GEO2-2115. Department of Innovation and Environmental Sciences. Utrecht University.

Entekhabi, D., I. Rodriguez-Iturbe and R.L. Bras, 1992. Variability in large-scale water balance with land surface-atmosphere interaction. Journal of climate 5, 798-813.

EPIC (Erosion Productivity Impact Calculator), 1995. EPIC's user's guide. USDA/ARS, Grassland, Soil and Water Research. Laboratory, Temple, TX.

Guttal, V. and C. Jayaprakash, 2008. Changing skewness: an early warning signal of regime shifts in ecosystems. Ecology Letters 11, 450-460.

Houérou, Le, H.N., 1996. Climate change, drought and desertification. Journal of Arid Environments 34, 133-185.

Ives, A.R., 1995. Measuring resilience in stochastic systems. Ecological Monographs 65, 217-233.

Jong, de, K., 2009. PCRaster Version 2 Manual >> List of PCRaster Operators >> Accuthresholdflux, accuthresholdstate. Available on http://pcraster.geo.uu.nl/.

Karssenberg, D., 2006. Upscaling of saturated conductivity for Hortonian runoff modelling. Advances in Water Resources 29, 735-759.

Karssenberg, D. and M.F.P. Bierkens, 2010. The use of spatio-temporal correlation to forecast critical transitions. Faculty of Geosciences, Utrecht University.

May, R.M., 1977. Thresholds and breakpoints in ecosystems with a multiplicity of stable states. Nature 269, 471-476.

Noy-Meir, I., 1975. Stability of grazing systems: an application of predator-prey graphs. Journal of Ecology 63(2), 459-481.

Rietkerk, M., M.C. Boerlijst, F. van Langevelde, R. HilleRisLambers, J. van de Koppel, L. Kumar, H.H.T. Prins and A.M. de Roos, 2002. Self-Organization of Vegetation in Arid Ecosystems. The American Naturalist 160(4), 524-530.

Rietkerk M., F. van den Bosch and J. van de Koppel, 1997. Site-specific properties and irreversible vegetation changes in semi-arid grazing systems. OIKOS 80, 241-252.

Rietkerk, M., S.C. Dekker, P.C. de Ruiter and J. van de Koppel, 2004. Self-Organized patchiness and catastrophic shifts in ecosystems. Science 305, 1926-1929.

Scheffer, M., J. Bascompte, W.A. Brock, V. Brovkin, S.R. Carpenter, V. Dakos, H. Held, E.H. van Nes, M. Rietkerk and G. Sugihara, 2009. Early-warning signals for critical transitions. Nature 461(3), 53-59.

Schlessinger, W.H., J.F. Raynolds, G.L. Cunningham, L.F. Huenneke, W.M. Jarrell, R.A. Virginia & W.G. Whitford, 1990. Biological Feedbacks in Global Desertification. Science 4946(246), 1043-1048.

Stroosnijder, L., 1996. Modelling the effect of grazing on infiltration, runoff and primary production in the Sahel. Ecological Modelling 92, 79-88.

Schwanghart, W., 2009. Variogramfit.m; Fits different theoretical variograms to an experimental variogram. Published Nov 25, 2009 on http://www.mathworks.com/matlabcentral/fileexchange/25948. Updated 14 Oct 2010. File ID: #25948. © 2009 Wolfgang Schwanghart. © 2006 The MathWorks, Inc.

WEPP (Water Erosion Prediction Project), 1995. WEPP User summary and WEPP Technical documentation. USDA/ARS/NCRS/FS/BLM, National Soil Erosion Research. Laboratory, West Lafayette, IN.

Wissel, C., 1984. A universal law of the characteristic return time near thresholds. Oecologia 65, 101-107.

Appendices

A. Analytical derivation of interesting points in figure 3.1.

In this appendix it is demonstrated how the points marked in figure 3.1 can be obtained analytically.

1. At what vegetation densities are the equilibria situated in absence of grazers?
2. What is the maximum growth rate in absence of grazers and what is the vegetation density at this maximum?

$$\frac{dV}{dt} = rV(1 - \frac{V}{K})$$

1. At what vegetation densities are the equilibria situated in absence of grazers?

At equilibria:

$$\frac{dV}{dt} = rV(1 - \frac{V}{K}) = 0$$

So:

$$rV = 0$$

or:

$$1 - \frac{V}{K} = 0$$

Equilibria are situated at:

$$V = 0 \text{ and } V = K$$

2. What is the maximum growth rate in absence of grazers and what is the vegetation density at this maximum?

At maximum dV/dt:

$$\frac{d^2V}{dt^2} = 0$$

$$r - \frac{2rV}{K} = 0$$

Vegetation density at maximum:

$$V = \tfrac{1}{2}K$$

Fill in in original equation to get maximum growth rate:

$$\frac{dV}{dt} = \tfrac{1}{2}Kr - \frac{\tfrac{1}{4}K^2r}{K} = \tfrac{1}{2}Kr - \tfrac{1}{4}Kr = \tfrac{1}{4}Kr$$

B. Saturation functions

In this appendix the saturation functions used in WOTMOD are discussed and it is explained how one can obtain soil evaporation as function of vegetation density.

Two types of saturation functions are used in WOTMOD.

$$y(x) = \frac{qx^n}{a^n + x^n} \qquad (B1)$$

$$y(x) = \frac{q(x + ay_0)}{a + x} \qquad (B2)$$

Table B1.

Eq.	Eq. in text	y	x	q	n	a	y_0
B1	3	Transpiration	V	$S^u E_{max}$	1	β	-
B1	3	Grazing	V	g	2	α	-
B2	2	Evapotranspiration	V	$S^u E_{max}$	-	β	V_0
B2	6	Infiltration capacity	V	I_{max}	-	γ	I_0

Equation B1 is a generalized version of the Michaelis-Menten equation (Hill function; Boer, de, 2010). The function has the following properties: y(0)=0, y(a)=q/2 and y(∞)=q. Since y=q/2 at x=a, a is often called half-saturation constant. Figure B1 shows that the shape changes with n. In ecosystem dynamics, equation B1 is often revered to as Holling's type II and III functional response for n=1 and n=2 respectively (Boer, de, 2010). When using Holling's type III functional response in predator-prey models[14], one often assumes that when the prey population is small (from 0 to q, see figure B1) the predator has another more easily accessible source of food (called prey-switching; Dekker & Eppinga, 2007). In WOTMOD this implies that at low vegetation densities grazers migrate to other areas with more vegetation.

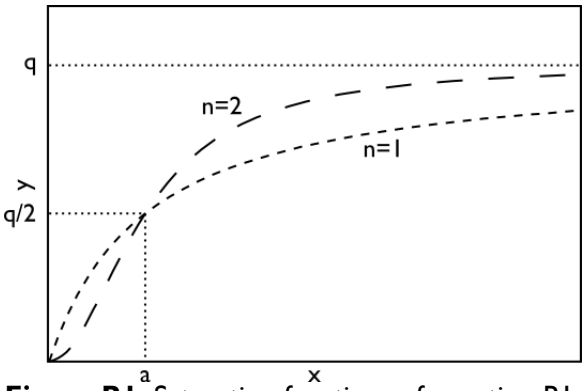

Figure B1. Saturation functions of equation B1.

[14] In this case: the predators are the grazers and the pray is the vegetation.

Equation B2 has the following properties, $y(0)=qy_0$, $y(a)=q(1+y_0)/2$ and $y(\infty)=q$. So instead of 0, this function starts at qy_0. This saturation function was used to relate infiltration capacity to vegetation density (as in Rietkerk et al., 1997). This function was also used to relate evapotranspiration to vegetation density, because soil evaporation continues when vegetation density is zero. Equations B3-B5 and figure B2 show how soil evaporation can be obtained from evapotranspiration and transpiration by plants.

$$E = S^u E_{max} \frac{V + \beta V_0}{V + \beta} \qquad \text{(B3)}$$

$$E_t = S^u E_{max} \frac{V}{V + \beta} \qquad \text{(B4)}$$

$$E_{soil} = E - E_t \qquad \text{(B5)}$$

In equation B2-B5, E is the evapotranspiration, E_t is transpiration by plants and E_{soil} is the evaporation from bare soil.

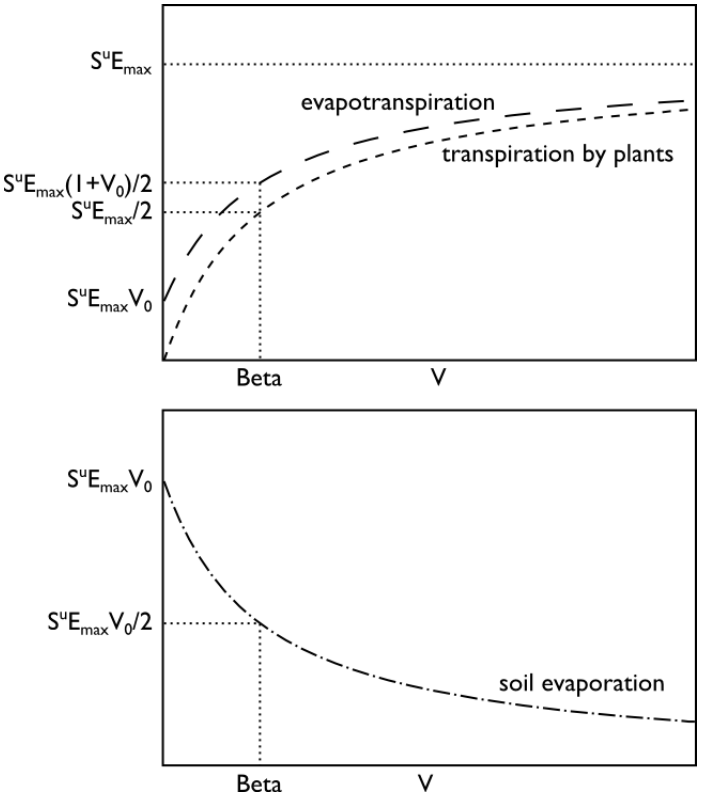

Figure B2. Evapotranspiration, transpiration (a) and soil evaporation (b) against vegetation density.

C. Matlab scripts
C.I. WOTMOD.m

Functions used in WOTMOD.m:
-numberofneighbors.m C.I.a.
-windowtotal.m C.I.b.
-accuthresholdfluxstate.m C.I.c.

```
clear all
close all

run='G';

%% Model properties

%size of map
m=100;              %height of map [cells]
n=100;              %width of map [cells]

%load/create ldd
ldd=ones(m,n)*2;    %parallel ldd
ldd(m,:)=5;
% load input/ldd.mat;

%calculate number of upstream cells
Upstream=(1:m)'*ones(1,n);

%length of model run
NrOfYears=2200;         %number of years [-]
NrOfWeeks=52;           %number of weeks [-]

%calculate number of neighbors
NrOfNB=numberofneighbors(m,n);

%create empty mapseries
Vmss=zeros(m,n,NrOfYears);
Smss=zeros(m,n,NrOfYears);
Qannmss=zeros(m,n,NrOfYears);

%create empty timeseries
Pann=zeros(NrOfYears,1);
ActFreq=zeros(NrOfYears,1);
ActMeanIntensity=zeros(NrOfYears,1);
Eventtype=zeros(NrOfYears,3);

%% Parameter values

%Soil parameters
por=0.4;            %porosity [-]
Zr=0.3;             %depth of rootzone [m]

%Precipitation parameters
MeanFreq=40;          %rain events per year (initial)
MeanIntensity=0.01;   %mean intensity (initial) [m/hour]
sdInt=0.0035;         %sd of intensity [m/hour]
```

```
load input/rndint.mat   %random values for calculating actual intensity
load input/rndevent.mat %random values for determining the occurrence of a rain event

%Infiltration
Imax=0.01;            %maximum infiltration capacity (at V=infinite) [m/hour]
gamma=0.75;           %scaling parameter to relate infiltration capacity to vegetation density [kg/m^2]
I0=0.05;              %infiltration capacity as fraction of Imax at V=0 [-]

%Evapotranspiration parameters
Emax=2;               %evaporation at V=infinite and S=1 [m/year]
V0=0.2;               %evaporation as fraction of Emax at V=0 [-]
beta=7;               %scaling parameter to relate evapotranspiration to vegetation density [kg/m^2]
u=0.5;                %relates S to evapotranspiration [-]

%Vegetation parameters
DV=0.2;               %dispersion rate of V [year^-1]
c=18;                 %water use efficiency [kg/m^2/m]
d=0.5;                %maintenance rate [year^-1]

sdW=1.5;              %sd of white noise on V [kg/m^2]
load input/dW.mat     %load white noise
dW=dW(1:m,1:n,1:NrOfYears);

%Grazing parameters
g=0.5;                %grazing rate (initial) [kg/m^2/year]
alpha=0.1;            %scaling parameter to relate grazing intensity to vegetation density [kg/m^2]

%Annual change in driver
gChange=0.002*g;                    %increase in grazing rate [kg/m^2/year/year]
freqChange=-0.0003*MeanFreq;        %decrease in mean rainfall frequency [1/year/year]
intChange=-0.00035*MeanIntensity;   %decrease in mean rainfall intensity [m/hour/year]

%Initial conditions
V=10*ones(m,n);               %initial biomass [kg/m^2]
S=0.1*ones(m,n);              %initial soil moisture [-]

%Minimum and maximum values for V and S
Vmin=0.001;
Smin=0.001;
Smax=1;

%% Dynamic section
for year=1:NrOfYears
   %add noise to vegetation density
   V=V+sdW*dW(:,:,year);
   V=max(V,Vmin);

   %print current timestep
   disp(year)

   %% Integrate over weeks
   for week=1:NrOfWeeks

      %calculate Icap
      Icap=Imax*(V+gamma*I0)./(V+gamma);

      %determine the occurrence of a rain event and calculate the its intensity
```

```
    ProbabilityOfRain=MeanFreq/NrOfWeeks;
    Intensity=0;                        %if there is no rainevent, the intensity is 0
    if rndevent(year,week)<ProbabilityOfRain
        %calculate rainfall intensity
        t=sdInt^2/MeanIntensity;            %scale parameter in gamma distribution
        k=(MeanIntensity/sdInt)^2;          %shape parameter in gamma distribution
        Intensity=gaminv(rndint(year,week),k,t);

        ActFreq(year)=ActFreq(year)+1;

        %determine type of rainevent
        Icapmax=max(Icap);
        Icapmin=min(Icap);
        if Icapmax<Intensity
            Eventtype(year,1)=Eventtype(year,1)+1;
        elseif Icapmin>Intensity
            Eventtype(year,3)=Eventtype(year,3)+1;
        else
            Eventtype(year,2)=Eventtype(year,2)+1;
        end
    end

    %calculate dS
    [Q,I]=accuthresholdfluxstate(Idd,Intensity,Icap);
    ET=(S.^u)*Emax.*(V+V0*beta)./(V+beta);
    dS=(I-ET/NrOfWeeks)/(Zr*por);

    %calculate dV
    Growth=c*(S.^u)*Emax.*V./(V+beta);
    Maintenance=d*V;
    Grazing=g*(V.*V)./((V.*V)+alpha*alpha);
    Dispersion=DV*(windowtotal(V,m,n)-NrOfNB.*V);
    dV=(Growth-Maintenance-Grazing+Dispersion)/NrOfWeeks;

    %add dV and dS to V and S
    V=V+dV;
    S=S+dS;

    %prevent negative values
    V=max(V,Vmin);
    S=max(S,Smin);
    S=min(S,Smax);

    %convert unit Q [m*cellarea/h]-->[m/h]
    Q=Q./Upstream;
    %calculate annual discharge and add to mapseries
    Qannmss(:,:,year)=Qannmss(:,:,year)+Q;
    %calculate annual precipitation and add to timeseries
    Pann(year)=Pann(year)+Intensity;
    %calculate actual mean intensity and add to timeseries
    ActMeanIntensity(year)=Pann(year)/ActFreq(year);


end

%get a map of V and S every year
Vmss(:,:,year)=V;
Smss(:,:,year)=S;
```

```
    %% change driver

    if year>200
        %increase in grazing rate
        g=g+gChange;

%         %decrease in frequency
%         MeanFreq=MeanFreq+freqChange;
%
%         %decrease in mean rainfall intensity
%         MeanIntensity=MeanIntensity+intChange;
    end

end

eval(['save results/model/mss',run,'.mat Vmss Smss Qannmss'])
eval(['save results/model/tss',run,'.mat ActFreq ActMeanIntensity Pann Eventtype'])
clear all
```

C.I.a. numberofneighbors.m

Calculates for every cell in a matrix of m by n the number of neighboring cells (min=2, max=4).

```
function [nrofnb]=numberofneighbors(m,n)
nrofnb=ones(m,n)*4;
nrofnb(1:m,1)=nrofnb(1:m,1)-1;
nrofnb(1,1:n)=nrofnb(1,1:n)-1;
nrofnb(1:m,n)=nrofnb(1:m,n)-1;
nrofnb(m,1:n)=nrofnb(m,1:n)-1;
```

C.I.b. windowtotal.m

Calculates for every cell in a matrix of m by n the sum of the values of its neighboring cells.

```
function tot=windowtotal(x,m,n)

xleft=zeros(m,n);
xright=zeros(m,n);
xtop=zeros(m,n);
xbottom=zeros(m,n);

xleft(:,2:n)=x(:,1:n-1);
xright(:,1:n-1)=x(:,2:n);
xtop(2:m,:)=x(1:m-1,:);
xbottom(1:m-1,:)=x(2:m,:);

tot=xleft+xright+xtop+xbottom;
```

C.I.c. accuthresholdfluxstate.m

Calculates the accumulation of material over a ldd. Transport only occurs if a threshold is exceeded.

```
function [sumflux,state]=accuthresholdfluxstate(ldd,material,threshold)

[m,n]=size(ldd);
sumflux=zeros(m,n);
state=zeros(m,n);
flux=ones(m,n);
while max(max(flux))>0
    cap=threshold-state;
    materialloss=min(material,cap);
    flux=material-materialloss;
    state=state+materialloss;
    sumflux=sumflux+flux;
    material=zeros(m,n);
    for i=1:m
        for j=1:n
            if flux(i,j)
                if ldd(i,j)==1
                    material(i+1,j-1)=material(i+1,j-1)+flux(i,j);
                elseif ldd(i,j)==2
                    material(i+1,j)=material(i+1,j)+flux(i,j);
                elseif ldd(i,j)==3
                    material(i+1,j+1)=material(i+1,j+1)+flux(i,j);
                elseif ldd(i,j)==4
                    material(i,j-1)=material(i,j-1)+flux(i,j);
                elseif ldd(i,j)==6
                    material(i,j+1)=material(i,j+1)+flux(i,j);
                elseif ldd(i,j)==7
                    material(i-1,j-1)=material(i-1,j-1)+flux(i,j);
                elseif ldd(i,j)==8
                    material(i-1,j)=material(i-1,j)+flux(i,j);
                elseif ldd(i,j)==9
                    material(i-1,j+1)=material(i-1,j+1)+flux(i,j);
                end
            end
        end
    end
end
```

C.II. analysis.m

Functions used in this script:

- semivar.m	C.II.a.
- mat2vec.m	C.II.b.
- variogramfit.m	(Schwanghart, W., 2009)
- skewtss.m	C.II.c.
- variancetss.m	C.II.d.
- corrtss.m	C.II.e.

```
clear all

%% Load files
disp ('Loading files')
run='G';
hmax=30;
window=200;

%Load matrix
eval(['load results/model/mss',run,'.mat'])
mat=Vmss;

%randomly select/load sample points
% SamplePoints=100;
% SamplePoints=fix(rand(1,nrofSamplePoints)*m*n+1);
load input/1percSamplePoints100x100.mat
load input/1percSamplePoints60x60.mat
nrofSamplePoints=size(SamplePoints,2);

%% Map Analysis + Storage of tss at Sample Points
disp ('Analysing maps + Storing tss at Sample Points')

%get number maps+size of matrix
[m,n,nrofmaps]=size(mat);
%predefine matrices&vectors
SemivarAllDir=zeros(hmax+1,3,nrofmaps);
SemivarXDir=zeros(hmax+1,3,nrofmaps);
SemivarYDir=zeros(hmax+1,3,nrofmaps);
skewmaptss=zeros(nrofmaps,1);
varmaptss=zeros(nrofmaps,1);
corrallmaptss=zeros(nrofmaps,3);
corrxmaptss=zeros(nrofmaps,3);
corrymaptss=zeros(nrofmaps,3);
rangeallmaptss=zeros(nrofmaps,1);
rangexmaptss=zeros(nrofmaps,1);
rangeymaptss=zeros(nrofmaps,1);
sillallmaptss=zeros(nrofmaps,1);
sillxmaptss=zeros(nrofmaps,1);
sillymaptss=zeros(nrofmaps,1);
sampletss=zeros(nrofmaps,nrofSamplePoints);

for curstep=1:nrofmaps

matcur=mat(:,:,curstep);
%calculate semivariance of map in x,y&xy direction
[SemivarAllDir(:,:,curstep),SemivarXDir(:,:,curstep),SemivarYDir(:,:,curstep)]=semivar(mat(:,:,curstep),hmax);
```

```
%enroll matrix into a vector (to calculating skewness and variance of map)
matvec=mat2vec(mat(:,:,curstep));

%calculate skewness of map
skewmaptss(curstep)=skewness(matvec);

%calculate variance of map
varmaptss(curstep)=var(matvec);

%calculate correlation of map in x,y&xy direction for h=1,2&3 cell lengths
corrallmaptss(curstep,:)=1-SemivarAllDir(2:4,2,curstep)/varmaptss(curstep);
corrxmaptss(curstep,:)=1-SemivarXDir(2:4,2,curstep)/varmaptss(curstep);
corrymaptss(curstep,:)=1-SemivarYDir(2:4,2,curstep)/varmaptss(curstep);

%calculate range&sill of map for x,y&xy direction
[rangeallmaptss(curstep),
sillallmaptss(curstep)]=variogramfit(SemivarAllDir(:,1,curstep),SemivarAllDir(:,2,curstep),[],[],SemivarAllDir(:,3,c
urstep),'plotit',false);
[rangexmaptss(curstep),
sillxmaptss(curstep)]=variogramfit(SemivarXDir(:,1,curstep),SemivarXDir(:,2,curstep),[],[],SemivarXDir(:,3,curst
ep),'plotit',false);
[rangeymaptss(curstep),
sillymaptss(curstep)]=variogramfit(SemivarYDir(:,1,curstep),SemivarYDir(:,2,curstep),[],[],SemivarYDir(:,3,curst
ep),'plotit',false);

bin=0.1;
matmax=8;
x=0:bin:matmax;
freq(1:matmax/bin+1,curstep)=histc(matvec,x)/(m*n);

%get cell values at sample points
for i=1:nrofSamplePoints
    sampletss(curstep,i)=matcur(SamplePoints(i));
end

end

%% Sampletss Analysis
disp ('Analysing tss of samplepoints')
[skewnesstss,meanskewtss,timetss]=skewtss(sampletss,window);
[vartss,meanvartss,timetss]=variancetss(sampletss,window);
[corrtss1,meancorrtss1,timetss]=corrtss(sampletss,window,1);
[corrtss2,meancorrtss2,timetss]=corrtss(sampletss,window,2);
[corrtss3,meancorrtss3,timetss]=corrtss(sampletss,window,3);


%% rename variables
disp ('Renaming variables')

eval(['SemivarAllDir' ,run, '= SemivarAllDir;'])
eval(['SemivarXDir' ,run, '= SemivarXDir;'])
eval(['SemivarYDir' ,run, '= SemivarYDir;'])

eval(['skewmaptss' ,run, '= skewmaptss;'])
eval(['varmaptss' ,run, '= varmaptss;'])
eval(['corrallmaptss' ,run, '= corrallmaptss;'])
```

```
eval(['corrxmaptss' ,run, '= corrxmaptss;'])
eval(['corrymaptss' ,run, '= corrymaptss;'])
eval(['rangeallmaptss' ,run, '= rangeallmaptss;'])
eval(['rangexmaptss' ,run, '= rangexmaptss;'])
eval(['rangeymaptss' ,run, '= rangeymaptss;'])
eval(['sillallmaptss' ,run, '= sillallmaptss;'])
eval(['sillxmaptss' ,run, '= sillxmaptss;'])
eval(['sillymaptss' ,run, '= sillymaptss;'])

eval(['freq' ,run, '= freq;'])

eval(['sampletss' ,run, '= sampletss;'])
eval(['timetss' ,run, '= timetss;'])
eval(['meanskewtss' ,run, '= meanskewtss;'])
eval(['skewnesstss' ,run, '= skewnesstss;'])
eval(['meanvartss' ,run, '= meanvartss;'])
eval(['vartss' ,run, '= vartss;'])
eval(['meancorrtss1' ,run, '= meancorrtss1;'])
eval(['corrtss1' ,run, '= corrtss1;'])
eval(['meancorrtss2' ,run, '= meancorrtss2;'])
eval(['corrtss2' ,run, '= corrtss2;'])
eval(['meancorrtss3' ,run, '= meancorrtss3;'])
eval(['corrtss3' ,run, '= corrtss3;'])



%% Save tss + semivariograms
disp ('Saving tss and semivariograms')
eval(['save results/analysis/semivar',run,'.mat SemivarAllDir',run,' SemivarXDir',run,' SemivarYDir',run])
eval(['save results/analysis/maptss',run,'.mat skewmaptss',run,' varmaptss',run,' corrallmaptss',run,'
corrxmaptss',run,' corrymaptss',run,' rangeallmaptss',run,' rangexmaptss',run,' rangeymaptss',run,'
sillallmaptss',run,' sillxmaptss',run,' sillymaptss',run])
eval(['save results/analysis/freq',run,'.mat freq',run])
eval(['save results/analysis/sampletss',run,'.mat sampletss',run,' timetss',run,' meanskewtss',run,'
skewnesstss',run,' meanvartss',run,' vartss',run,' meancorrtss1',run,' corrtss1',run,' meancorrtss2',run,'
corrtss2',run,' meancorrtss3',run,' corrtss3',run])

disp ('Finished!')
clear all
```

C.II.a. semivar.m

Calculates the semivariance in x, y and xy direction.

```
function [semxy,semx,semy]=semivar(x,hmax)
[m,n]=size(x);

q=1;
semvary=zeros(hmax+1,1);
semvarx=zeros(hmax+1,1);
numbery=zeros(hmax+1,1);
numberx=zeros(hmax+1,1);
qy=1;
qx=1;

%horizontaal, verticaal & diagonaal (lb-ro)
for dx=0:hmax
   for dy=0:hmax
      hcheck=(dx^2+dy^2)^0.5;
      if hcheck<(hmax+0.5)
         hmess(q)=hcheck;
         sqdiff(q)=sum(sum((x(1:m-dy,1:n-dx)-x(1+dy:m,1+dx:n)).^2));
         nrmess(q)=(m-dy)*(n-dx);
         if dx==0
            numbery(qy)=nrmess(q);
            semvary(qy)=sqdiff(q)/numbery(qy)/2;
            qy=qy+1;
         end
         if dy==0
            numberx(qx)=nrmess(q);
            semvarx(qx)=sqdiff(q)/numberx(qx)/2;
            qx=qx+1;
         end
         q=q+1;
      end
   end
end

%diagonaal (lo-rb)
for dx=1:hmax
   for dy=1:hmax
      hcheck=(dx^2+dy^2)^0.5;
      if hcheck<(hmax+0.5)
         hmess(q)=hcheck;
         sqdiff(q)=sum(sum((x(1+dy:m,1:n-dx)-x(1:m-dy,1+dx:n)).^2));
         nrmess(q)=(m-dy)*(n-dx);
         q=q+1;
      end
   end
end

%sorteren
hroundmess=round(hmess);
number=zeros(hmax+1,1);
semvar=zeros(hmax+1,1);
h=zeros(hmax+1,1);
```

```
for i=0:hmax
    number(i+1)=sum(nrmess.*(hroundmess==i));
    sumsqdiff=sum(sqdiff.*(hroundmess==i));
    semvar(i+1)=sumsqdiff/number(i+1)/2;
    h(i+1)=i;
end

semxy=[h,semvar,number];
semx=[h,semvarx,numberx];
semy=[h,semvary,numbery];
```

C.II.b. mat2vec.m

Creates a vector (one by mxn) out of a matrix (m by n).

```
function vec=mat2vec(mat)
[m,n]=size(mat);
vec=zeros(1,m*n);
q=1;
for i=1:m
   for j=1:n
      vec(q)=mat(i,j);
      q=q+1;
   end
end
```

C.II.c. skewtss.m

Calculates the (mean) skewness over time of multiple timeseries using a moving window.

```
function [s,smean,time]=skewtss(vec,window)
[nrofsteps,nrofSamplePoints]=size(vec);

time=window:1:nrofsteps;
s=zeros(nrofsteps-window,nrofSamplePoints);

for i=1:nrofsteps-window+1
    s(i,:)=skewness(vec(i:i+window-1,:));
end

smean=mean(s,2);
```

C.II.d. variancetss.m

Calculates the (mean) variance over time of multiple timeseries using a moving window.

```
function [s,smean,time]=variancetss(vec,window)
[nrofsteps,nrofSamplePoints]=size(vec);

time=window:1:nrofsteps;
s=zeros(nrofsteps-window,nrofSamplePoints);

for i=1:nrofsteps-window+1
    s(i,:)=var(vec(i:i+window-1,:));
end

smean=mean(s,2);
```

C.II.e. corrtss.m

Calculates the (mean) correlation over time of multiple timeseries using a moving window.

```
function [s,smean,time]=corrtss(vec,window,h)
[nrofsteps,nrofSamplePoints]=size(vec);

time=window:1:nrofsteps;
s=zeros(nrofsteps-window,nrofSamplePoints);

for i=1:nrofsteps-window+1
    v=vec(i:i+window-1-h,:);
    vplus=vec(i+h:i+window-1,:);
    meanv=ones(window-h,1)*mean(v);
    meanvplus=ones(window-h,1)*mean(vplus);
    s(i,:)=mean((v-meanv).*(vplus-meanvplus))./(std(v,1).*std(vplus,1));
end

smean=mean(s,2);
```

D Shape of gamma probability density functions with different means and equal variance.

In this appendix it is explained how decreasing the mean rainfall intensity affects the shape of the probability distribution for rainfall intensity.

Rainfall intensity is modelled using the gamma probability density function:

$$f(x;k,t) = x^{k-1}\frac{e^{-x/t}}{t^{k}\Gamma(k)} \qquad \text{(D1)}$$

In equation D1, t is the scale parameter, k is the shape parameter and x is the gamma distributed random variable (rainfall intensity in WOTMOD).
The shape and scale parameter can be expressed in terms of mean and variance: $\sigma_{Int}=k^{1/2}\cdot t$ and $\mu_{Int}=k\cdot t$, from which follows: $t=\sigma_{Int}^2/\mu_{Int}$ and $k=(\mu_{Int}/\sigma_{Int})^2$. This implies that changing the mean while keeping the standard deviation constant (as in WOTMOD), affects both scale and shape of the gamma pdf. This is illustrated in figure D1.

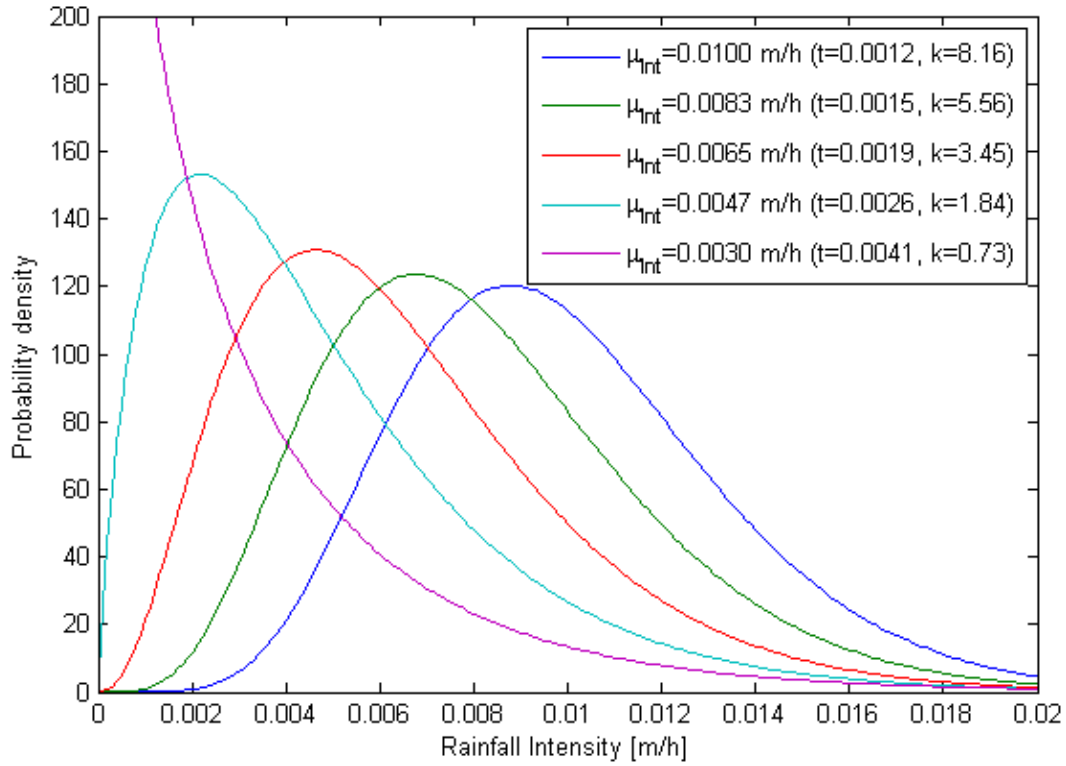

Figure D1. Gamma distribution for different mean rainfall intensities.

E Extra figures for chapter 4

E.I. Model Behaviour

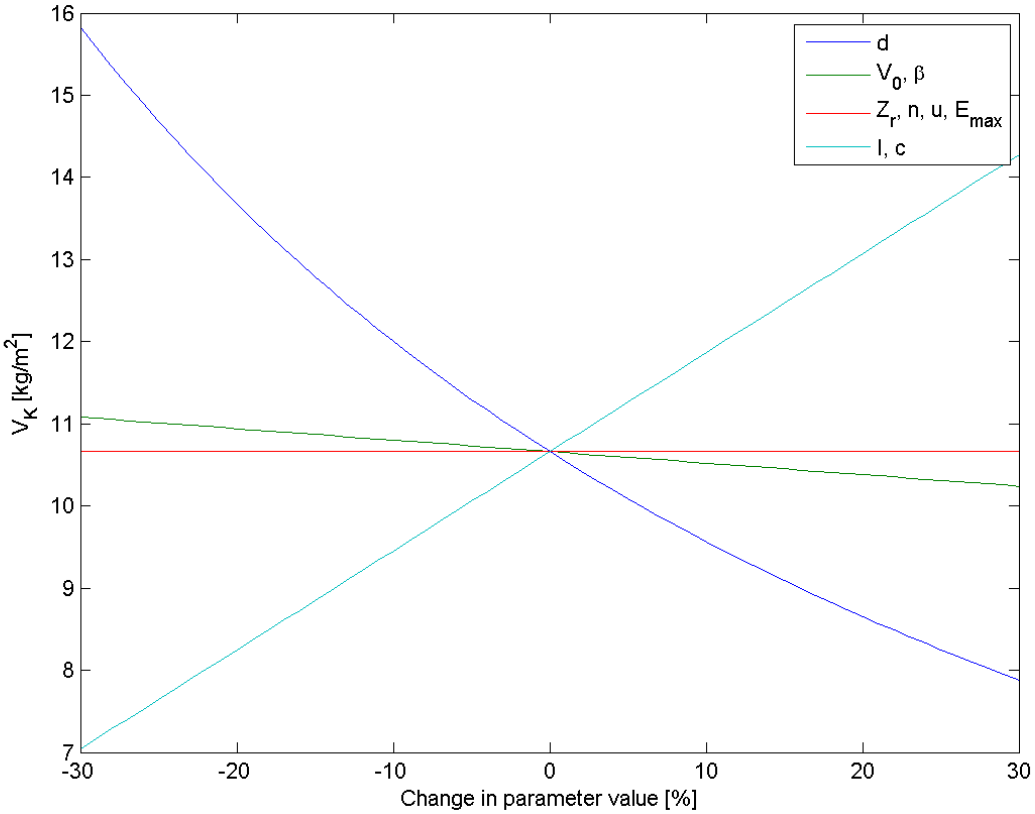

Figure E1. Carrying capacity [kg/m^2] for different parameter settings.

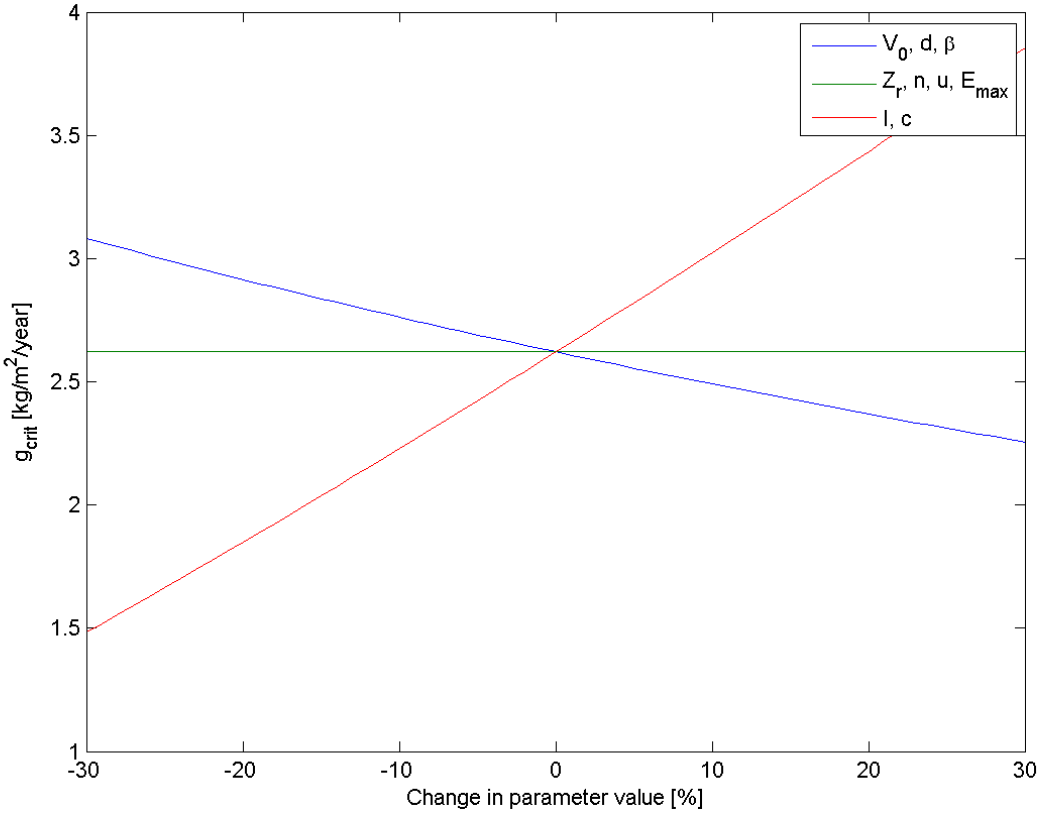

Figure E2. Maximum growth rate or grazing rate at transition [kg/m^2/year] for different parameter settings.

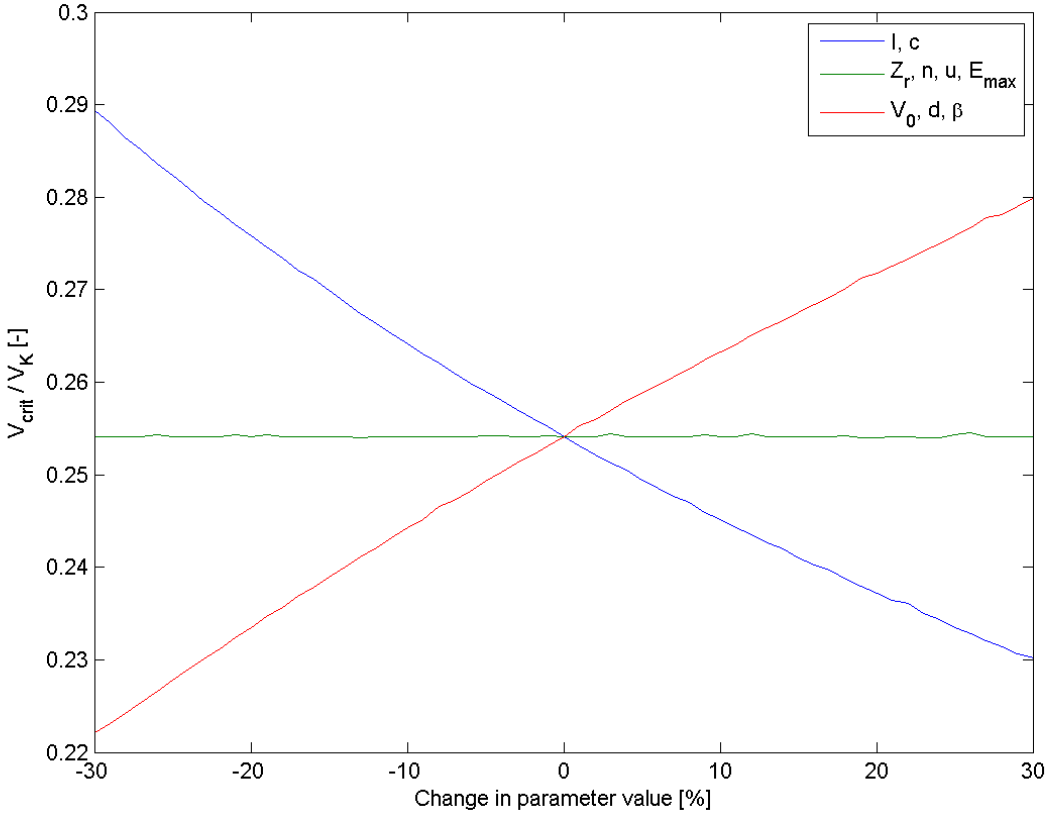

Figure E3. Asymmetry in growth curve (0.5 if symmetrical) for different parameter settings.

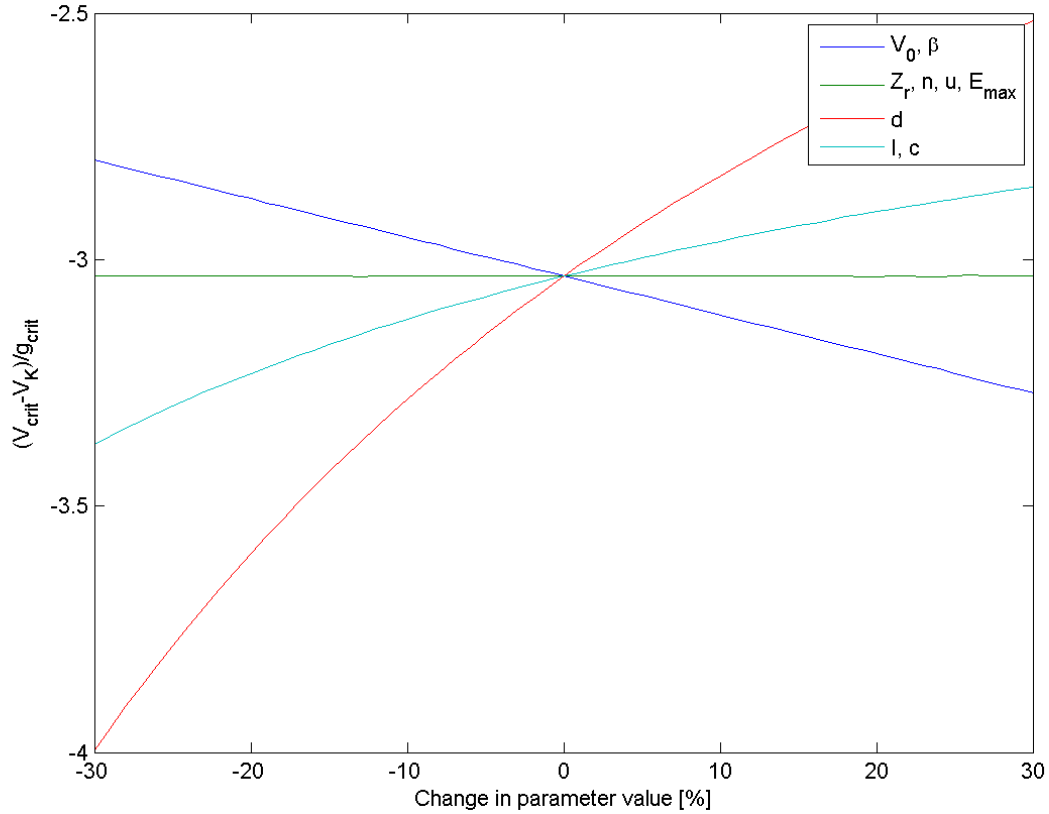

Figure E4. Average slope in vegetation density till transition or sensitivity of vegetation density to grazing for different parameter settings.

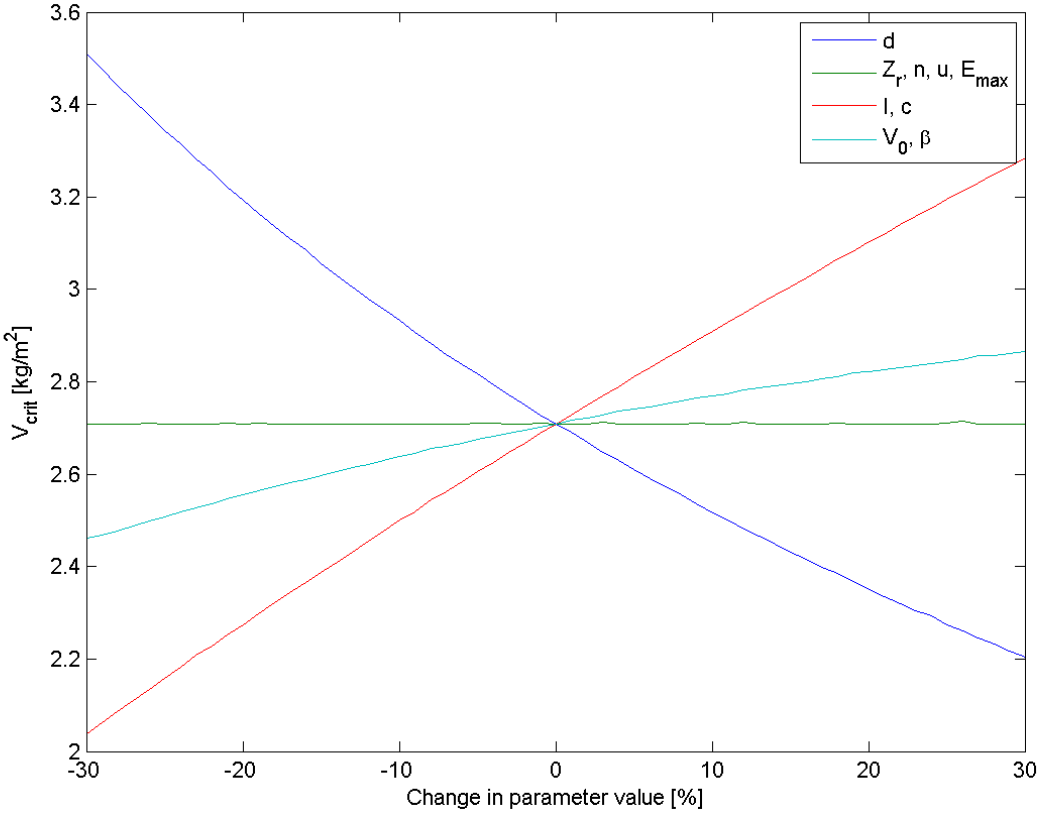

Figure E5. Vegetation density at maximum growth rate or vegetation density at transition for different parameter settings.

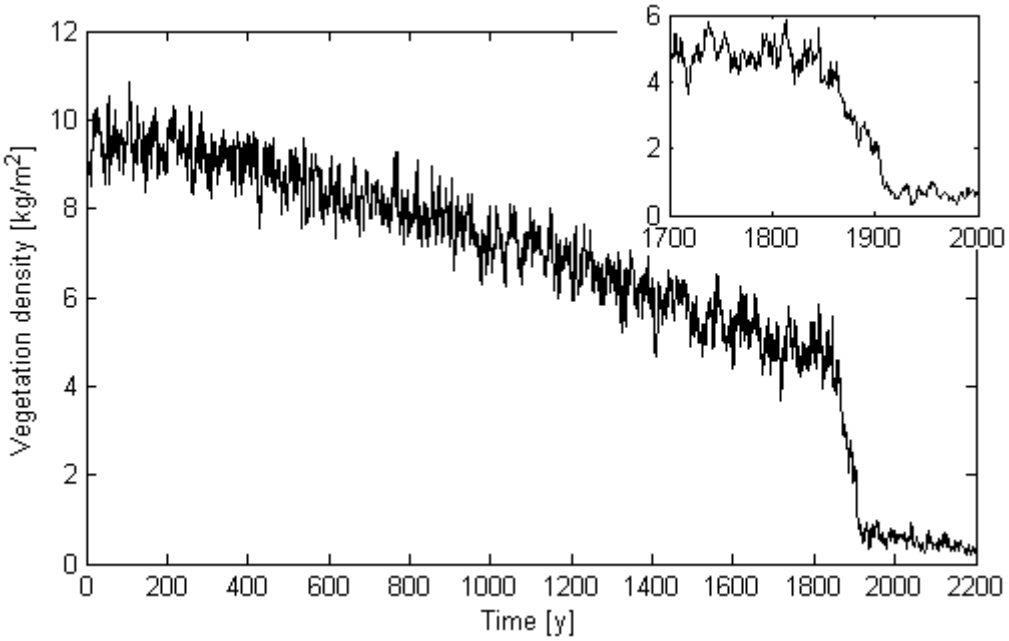

Figure E6. Map averaged vegetation density over time. Perturbations are mainly caused by the stochastically modelled rainfall, as the white noise on the vegetation density is averaged out. The transition is 'paused' for about 30 years because vegetation patches form.

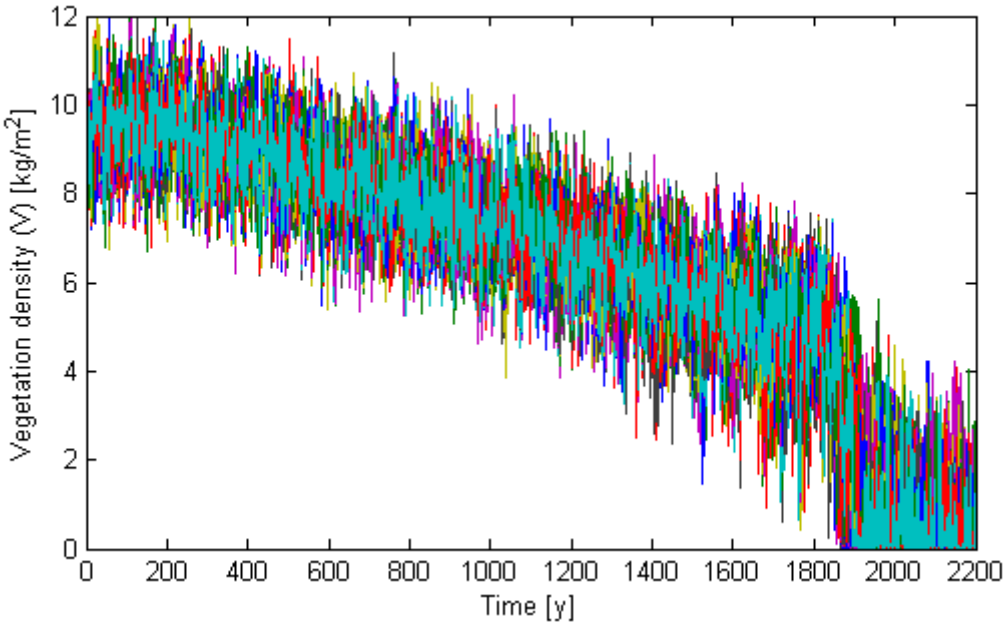

Figure E7. Vegetation density at sample cells over time.

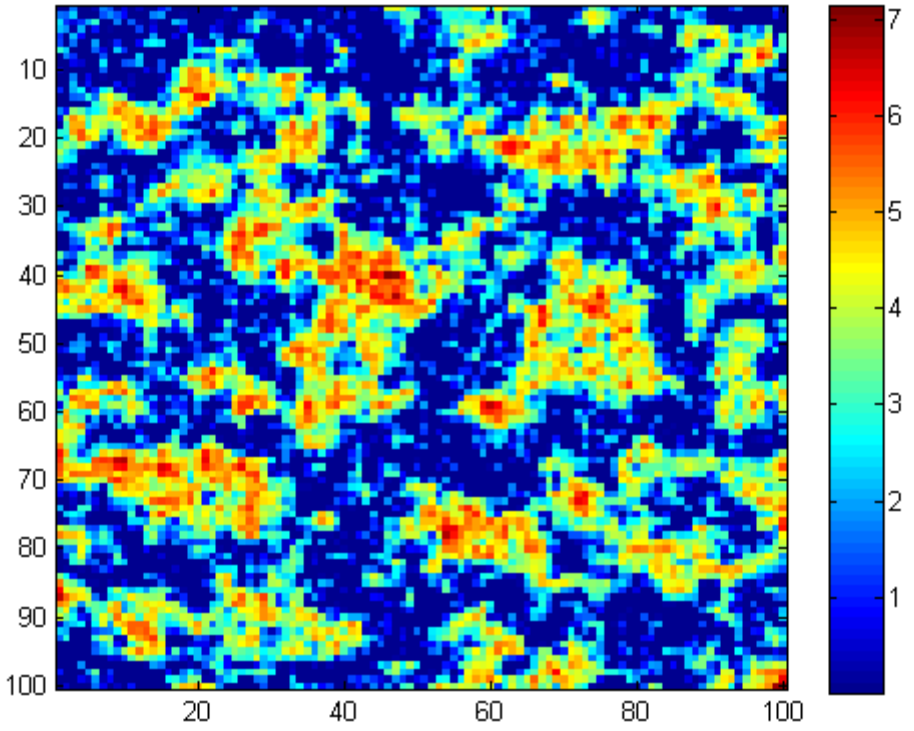

Figure E8. Map of vegetation density [kg/m^2] at t=1900 y.

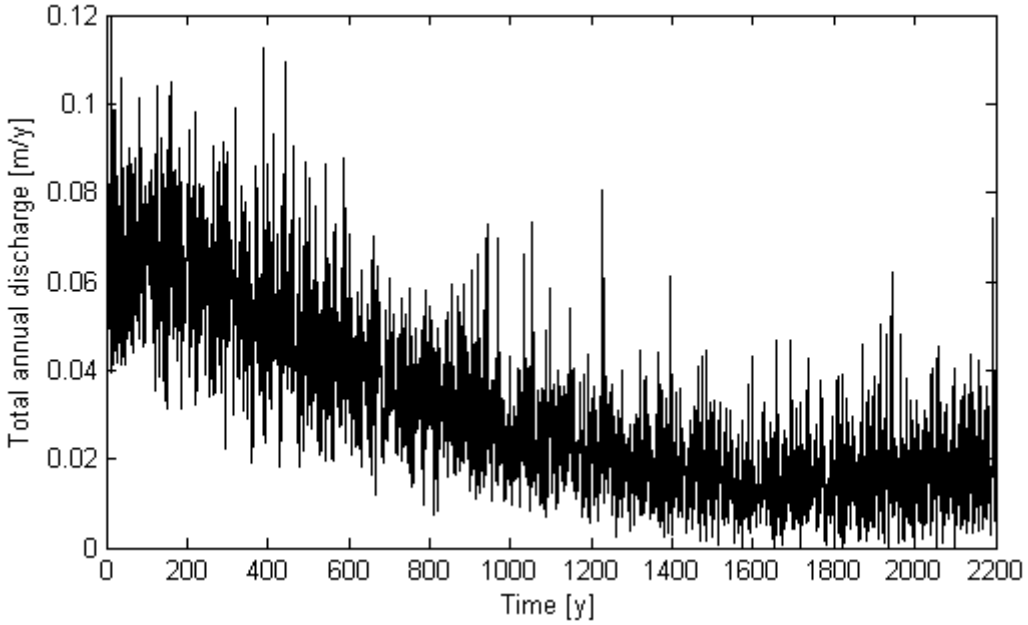

Figure E9. Total annual discharge from the modelled area in scenario Int.

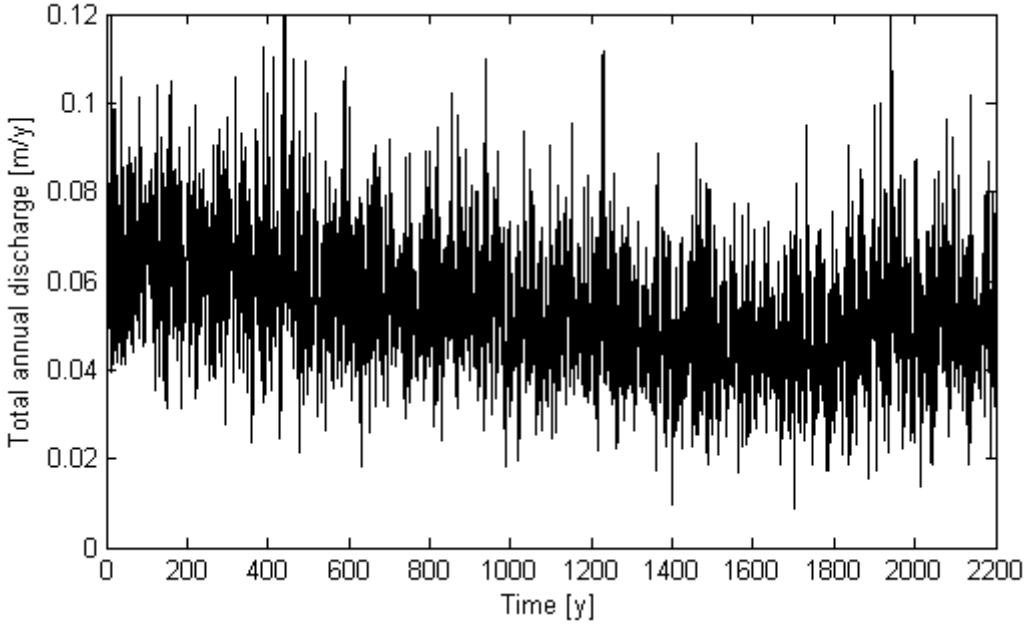

Figure E10. Total annual discharge from the modelled area in scenario Freq.

E.II. Early warning signals

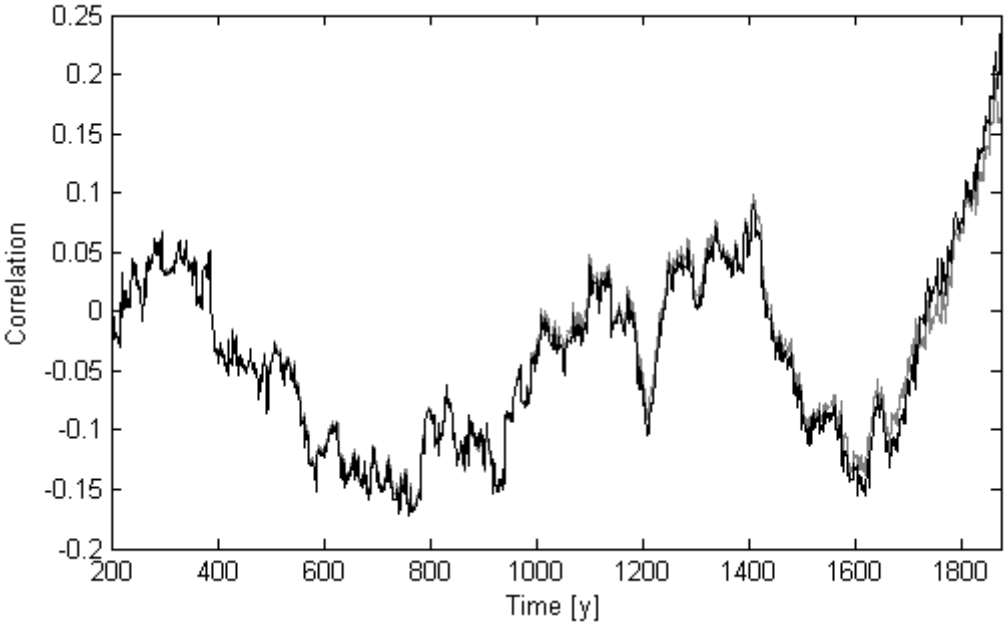

Figure E11. Average lag-1-autocorrelation in annual discharge at sample points till transition time (t=1875y). Number of sample points= 100, window=200. Grey: scenario 0, black: scenario G. There is no increase in autocorrelation in annual discharge for scenario G compared to scenario 0.

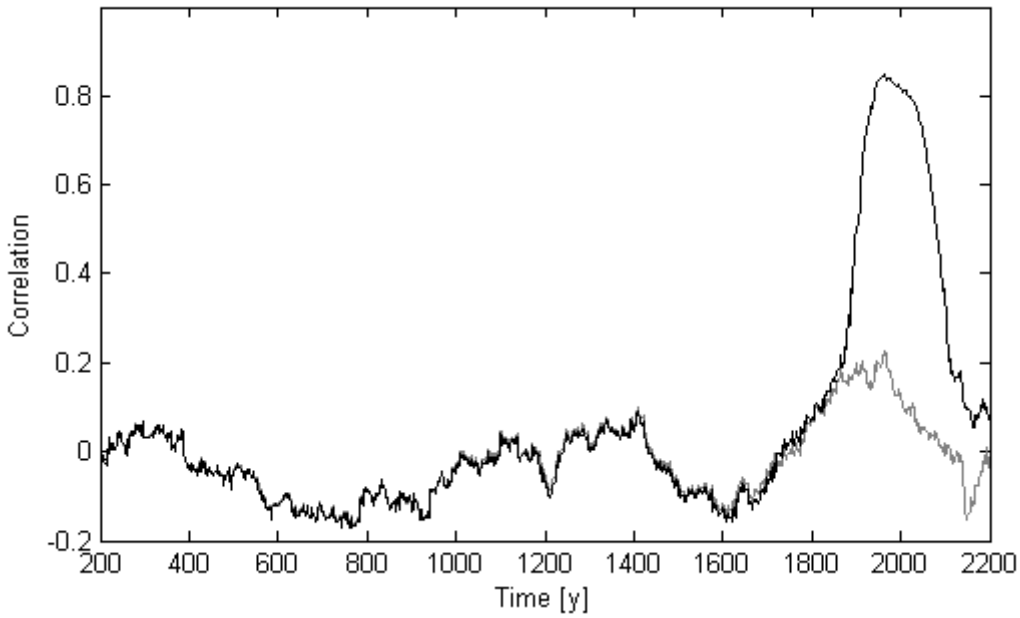

Figure E12. Average lag-1-autocorrelation in annual discharge at sample points till t=2200y. Number of sample points=100, window=200. Grey: scenario 0, black: scenario G. During the transition the autocorrelation increases in scenario G.

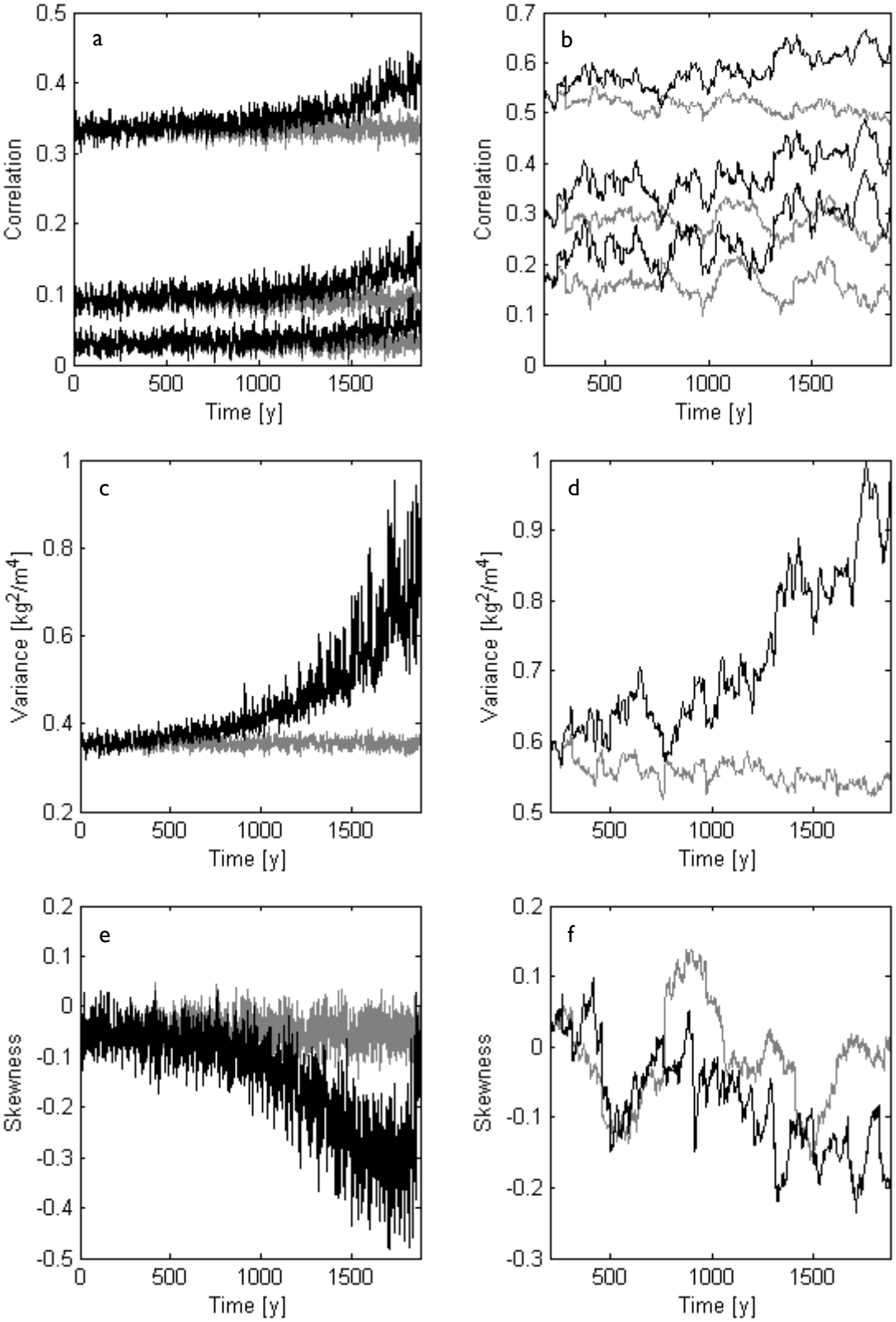

Figure E13. Spatial (left) and temporal (right) signals in vegetation density for scenario Freq. In grey scenario 0, in black: scenario Int. For a and b: h=1, 2 and 3 cell lengths/years.

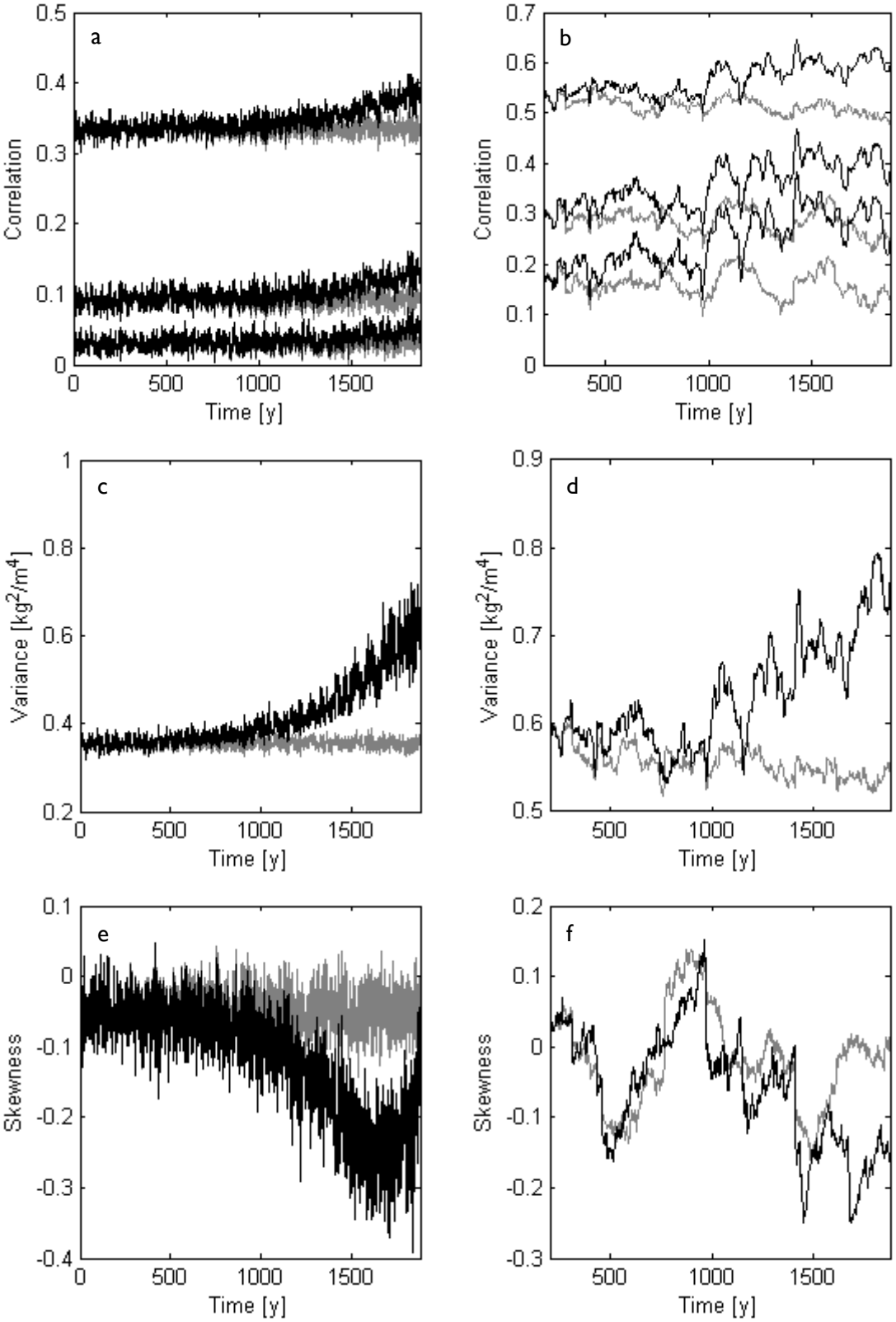

Figure E14. Spatial (left) and temporal (right) signals in vegetation density for scenario Int. In grey scenario 0, in black: scenario Int. In a and b: h=1, 2 and 3 cell lengths/years.

E.III. Additional runs

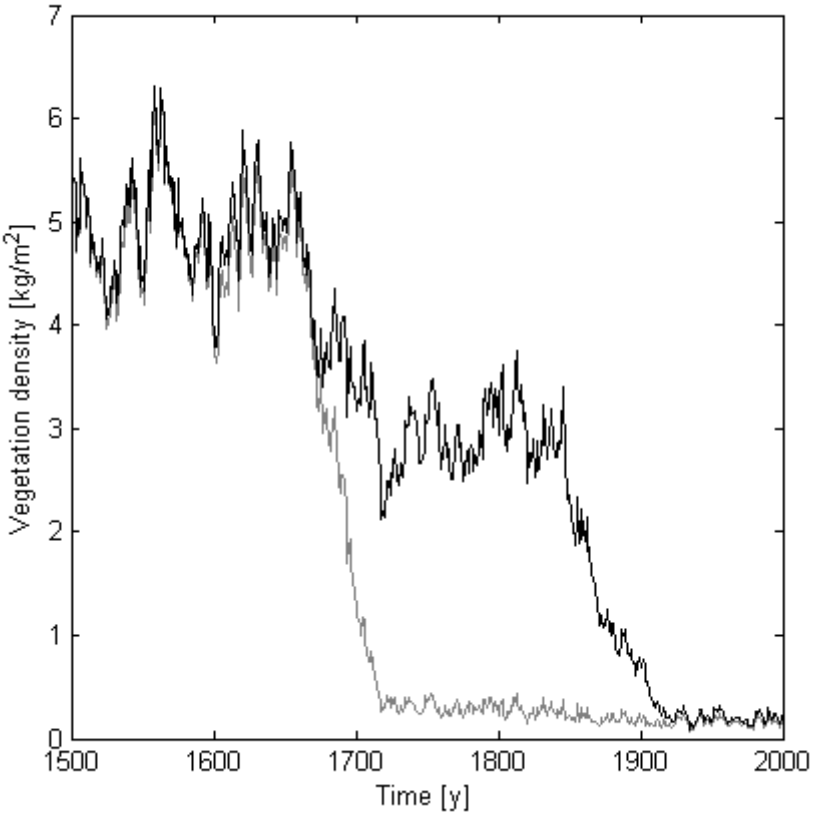

Figure E15. Map averaged vegetation density with I_0=0.05. In grey: runoff generation "switched off."

F Extra figures for chapter 5

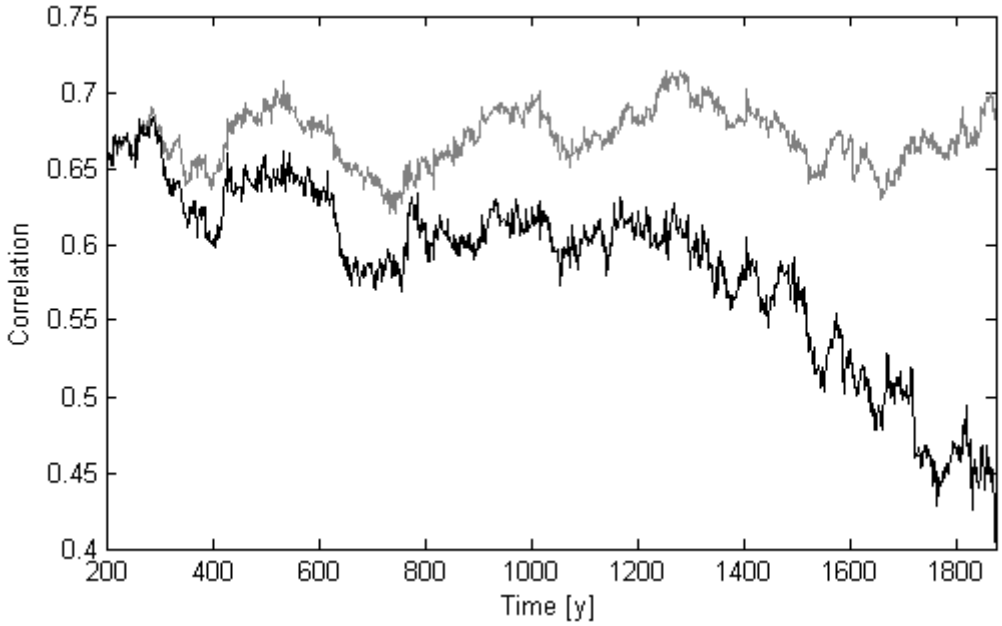

Figure F1. Correlation between annual precipitation and map averaged vegetation density against time (window: 200 years).